PREPARATION AND EVALUATION OF A 3D LIVER TUMOR SPHEROID MODEL VIA THE USE OF A COMPOSITE COLLAGEN AND POLYMER HYDROGEL

MARTIN NURMIK

(B.Sc (Hons.), University of Manchester)

A THESIS SUBMITTED

FOR THE DEGREE OF MASTER OF SCIENCE

DEPARTMENT OF PHARMACY

NATIONAL UNIVERSITY OF SINGAPORE

2016

DECLARATION

I hereby declare that this thesis is my original work and it has been written by me in its entirety. I have duly acknowledged all the sources of information which have been used in the thesis.

This thesis has also not been submitted for any degree in any university previously.

_____

Martin Nurmik

14 February 2016

Acknowledgments

Firstly I would like to thank my supervisor, Assoc. Prof. Yi Yan Yang. Without her I would probably have never had the chance to come to Singapore and her guidance and encouragement has been immensely helpful for me over the past year and a half, in far more areas than just my thesis work.

I am also very grateful to A*STAR for funding my studies in NUS and whose support structure has allowed me to continue working on my project without any issues. More specifically I would like to thank everyone at the Institute of Bioengineering and Nanotechnology. Never did I feel unneeded or shunned and everyone in the institute always had encouraging words to push me forwards. The friendliness and humor shown by everyone were what kept me going and what made IBN a truly special place to work.

To list and mention all the help I got from members of our lab group would inflate this section to far longer than a page, so I'll try to keep things brief. Thank you, everyone! Thank you for showing me the ropes when I first came to the lab, thank you for giving me advice when I was stumped, thank you for everything! My special thanks go to Jeremy, Majad and Ashlynn for helping me proof-read and improve my thesis and to Xiyu, Jye Yng, David, and Victor for aiding me with the various lab-related aspects of my project.

My thanks also go to all the lecturers and staff in NUS. Over the past year and a half, I have learned and experienced many new things, much of it specifically thanks to everyone in NUS. The teaching I have received here is truly exceptional and I am extremely grateful for all I have learned in NUS.

Lastly, and very importantly, I would like to thank my family and friends back home who supported me for the entirety of my stay here in Singapore. For listening to me when I was sad and for sharing my joy when I was happy. Even though the distance between us was vast, it nevertheless felt like you were just there, around the corner and I could always call you if I needed it.

Thank you.

Table of Contents

Summary

Over the past decade, there has been an exponential increase in both the number and complexity of various anti-tumor therapies and drugs. These developments, in turn, have necessitated the development of a three-dimensional tumor tissue model that could adequately replicate the *in vivo* tumor environment. While various different models have been suggested, the vast majority of them rely on the use of natural biomaterials, such as type I collagen and Matrigel, to provide an environment that can mimic cell-ECM interactions. However, weaknesses such as high cost and mechanical inflexibility, remain large stumbling blocks. Using hydrogels formed out of both PEG-based triblock co-polymers (Poly(MTC-VitE)1.25-PEG10k-Poly(MTC-VitE1.25), Poly(MTC-VitE)2.5-PEG10k-Poly(MTC-VitE)2.5 and Poly(MTC-OBn)8.5 -PEG8k-Poly(MTC-OBn)8.5) and type I collagen, a number of three-dimensional (3D) matrices were prepared for tumor spheroid growth. The 3D matrices were characterized for hydrogel clarity (using visual observations and imaging), tumor spheroid growth (using measurements obtained via light microscopy), permeability (using confocal imaging of doxorubicin penetration) and rheological stiffness (using rheometry data), for their potential use as three-dimensional tumor models. What we found was that while certain types of our composite hydrogels showed lower levels of overall spheroid growth when compared with the control, one polymer (Poly(MTC-VitE)1.25-PEG10k-Poly(MTC-VitE1.25)) showed almost identical levels of spheroid growth to those found in the collagen control, while possessing a high flexibility in terms of mechanical attributes, such as stiffness. However, certain aspects, such as anti-cancer drug permeability, remain key issues that must be examined more thoroughly in further studies.

List of Tables

List of Figures

1. Introduction

1.1 Tumor research in the modern world

Cancer is one of the most important medical challenges currently facing modern mankind. Cancers are a large group of diseases that are mainly characterized by the mutation of normal cells into invasive, highly replicative tumorigenic cells. Via a process called metastasis, these cancerous cells can then spread to other organs, causing extensive systemic damage to the human body, which typically culminates in the death of the patient. According to the World Health Organization, cancerous diseases were responsible for approximately 8.2 million deaths in 2012, the highest of any non-transmissible disease, and the number of new cases is expected to rise by over 70%, to 22 million, over the course of the next two decades. Furthermore, the economic costs of various tumorigenic diseases are staggering, as seen from the fact that only the direct medical costs of cancer treatment in the United States accounted for 88 billion dollars in 2011, while reduction in productivity due to premature cancer mortality in Europe was estimated to account for a loss of 75 billion euros **[1]**. Therefore, research into potential therapies or avenues of treatment is of absolutely vital importance from both a moral and a fiscal standpoint.

However, due to its polygenic and multifactorial nature, complete treatment of cancer still remains a task of almost herculean difficulty. Traditional approaches, such as chemo and radiotherapy, have significant downsides, typically associated with systemic toxicity and death of other rapidly dividing cells, such as hair follicle cells or hematopoietic cells in the bone marrow. In addition, drug resistance remains an issue, even with extremely broad target approaches such as chemotherapy. Cellular mechanics, such as drug efflux

through the ATP-binding cassette transporter families and up-regulation of members of the DNA repair pathways, such as ERCC, serve as inducers of chemotherapeutic resistance in tumor cells **[2]**. Because of the systemic downsides of chemo and radiotherapy, more recent therapeutic approaches in cancer therapy have attempted to solve the problem by targeting cancer-specific mutations, typically occurring in various kinases. However, while very specific for tumor cells and with far less serious side effects, specific molecular targeting drugs (such as tyrosine kinase inhibitors) are still subject to the development of cancer resistance, albeit through different cellular mechanics than in the case of conventional therapies.

One key example of this is the incidence of resistance accompanying the Bcr-Abl tyrosine kinase inhibitor, Imatinib, in chronic myeloid leukemia (CML). While initially showing extremely promising results, it was shown that a sizable proportion of the chronic myeloid leukemia patients were at risk of primary or secondary Imatinib resistance **[3]**, via mutations in the target of Imatinib, BCL-ABL1 **[2]**. While Imatinib is still widely used for the treatment of CML and "second generation" tyrosine kinase inhibitors (inhibitors which are capable of both suppressing the wild type and mutant Bcr-Abl) are now in use, resistance still remains a considerable issue with many single target therapies. Because of the massive difficulties involved in overcoming drug resistance, and due to significant differences between different tumor variations, creating viable and easily applicable *in vitro* tumor modeling systems has long been of great interest to the medical community.

1.2 2D tumor models

Most tumor-related drug and characterization studies are performed using two-dimensional cell culture models. These models typically involve cultivating a monolayer of tumor cells on the surface of a tissue culture plate. Tests involving 2D tumor models are relatively easy to set up and have been extensively used for both drug studies and also to characterize the nature and behavior of a variety of different tumor cell lines. However, while they are simple to use, 2D culture models suffer from a number of major drawbacks that greatly hamper their use in research and drug development.

One of the main key problems with 2D tumor cultures is their inability to induce neither cell to cell interactions between the tumor cells, nor cell to ECM interactions that take place between the tumor cells and the extracellular matrix. These interactions have been shown to have significant effects on a variety of different tumor cell characteristics such as drug metabolism, protein synthesis, differentiation and cell viability, and the lack of these characteristics has been shown to result in increased response to anti-cancer drugs, such as Paclitaxel **[4]**. Furthermore, it has been observed that in the case of organotypic neoplasias, the expression profile of various oncogenic signals differs greatly between two-dimensional tumor cultures and *in vivo* tumor tissue, further calling into question the ability of monolayer cultures to accurately mimic real tumor growth and behavior **[5]**.

1.3 3D tumor models

Therefore, to overcome the limitations associated with traditional two-dimensional tissue cultures, as well as to more accurately portray the natural cancers occurring in patients, a three-dimensional model capable of replicating the natural tumor environment is necessary. This, in itself, is not a particularly novel concept, as animal models, such as subcutaneous tumor xenografts in immunodeficient mice, have been used in medical studies for decades to prove the efficacy of various drugs and therapies. Unfortunately, animal trials have always been subject to a significant degree of uncertainty, due to significant biological differences between species commonly used for medical trials (such as mice) and humans. For example, subcutaneously induced tumors are rarely useful for characterizing anti-metastatic drugs, as subcutaneous xenografts very rarely metastasize in mice **[6]**. In addition to the biological difficulties involved, there are a considerable number of ethical issues involved with the use of animals in clinical research. And while several interesting approaches are being used to overcome many of the biological difficulties involved, such as "humanization" of mice via the use of genetic engineering **[7]**, it is unlikely that the ethical controversies surrounding the use of animals in clinical trials will truly ever disappear.

Due to these natural drawbacks associated with animal models, various *in vitro* three-dimensional (3D) tumor models have been proposed over the course of the past decade. Three-dimensional *in vitro* approaches can be broadly divided into variety of categories, most of which are based on the cultivation of tumor spheroids in media or focused around their encapsulation in a variety of ECM-mimicking environments, although other novel approaches, such as the use of cell printing to manufacture a 3D

scaffold, have also been suggested as potential alternative methods for *in vitro* tumor modeling **[4]**.

Multicellular tumor spheroids (MCTS) are aggregates of tumor cells within the 20 µm to 1 mm range **[4]** and are naturally formed when tumor cells are cultivated in non-adhesive or buoyant environments. Whilst growing, the spheroids will develop into a structure that is extremely reminiscent of natural tumors appearing in patients. A gradient of rapidly expanding cells forms the outer periphery of the spheroids while cells closer to the center form a so-called "hypoxic core". This hypoxic core is formed out of quiescent and necrotic cells and is characterized by low levels of oxygen, low levels of ATP distribution and a high degree of DNA strand breaks, as can be seen in *Figure 1*. This distribution of cell heterogeneity is extremely similar to that found in vascular micro-regions of tumors **[8]** and it has been clearly demonstrated that in MCTS display a significantly higher degree of drug resistance (typically referred to as multicellular resistance) than equivalent 2D models **[9].** Tumor spheroids can also be scaled up relatively easily (via the use of non-adhesive 96-well plates or spinner flask cultivation methods), making high throughput screening of spheroids an ever closer possibility in the future **[10].** However, several key problems remain with MCTS, most importantly the often variable size of the cultivated spheroids and the lack of cell-ECM interactions in standard, non-encapsulated MCTS cultures.

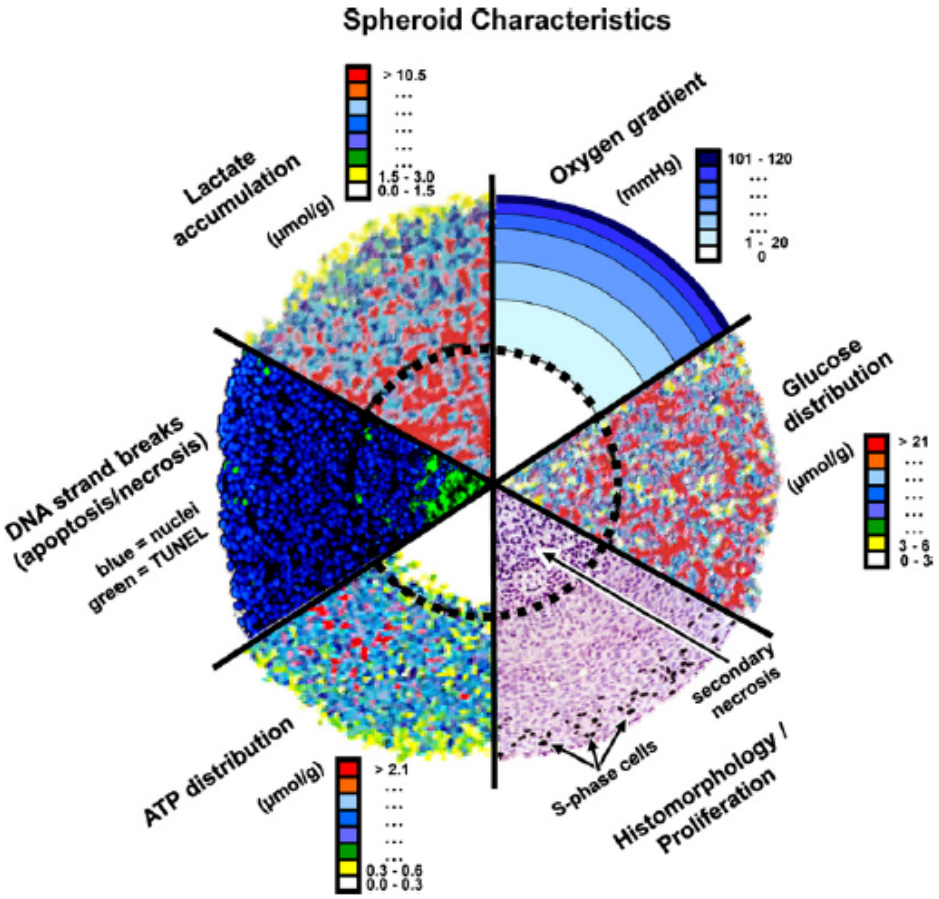

Figure 1 – Characteristics of tumor spheroids. An overview and characterization of ATP distribution, DNA strand breakage, lactate accumulation, oxygen and glucose distribution and histology within tumor spheroids. Figure taken from Hirschhaeuser, et al, 2010.

In an effort to overcome this limitation, several models have been developed, where the MCTS are placed in an ECM imitating environment. A variety of substances, both natural and synthetic have been tested for this purpose. Amongst these, natural biomaterials such as type I collagen and Matrigel are most commonly used, while various polyesters and polyethylene glycol (PEG) based polymers have also been extensively studied. Type I collagen, for example, is the most abundant type of collagen in the human body and is the most abundant ECM protein in most tissues. Collagen gels have been shown to be

capable of mimicking both loose and dense connective tissue, based on the collagen concentration **[11]** and liver tumor spheroids cultivated in collagen gels have been demonstrated to show a higher degree of doxorubicin resistance than standard, non-encapsulated MCTS **[12]**. Similar results have been demonstrated in hydrogels prepared from Matrigel, a mixture composed of a large variety of different ECM proteins and growth factors, produced from Engleberth-Holm-Swarm (EHS) mouse sarcoma cells. Matrigel has been widely used for subcutaneous tumor inoculation in mice and Matrigel hydrogels have been widely used to study the effect of 3D matrix factors on cellular processes such as the development of apoptotic resistance **[13]** and metastasis induced morphological and gene expression changes **[14]**.

Studies associated with synthetic polymers have been less successful, mainly due to the lack of bioactivity shown by man-made materials, in comparison to naturally derived biomaterials, such as type I collagen. Nevertheless, materials such as porous polyester scaffolds have been shown to possess *in vivo* mimetic angiogenic signaling **[15]** and tumor constructs cultivated in these models do show levels of hypoxia clearly resembling that of normal in vivo tumors found in patients **[16]**. However, due to the lack of natural bioactivity and the biological microenvironment (when compared to naturally derived three-dimensional models), tumor cell behavior in these synthetic models is extremely variable, greatly complicating their use as cancer models. It is therefore not an exaggeration to say that the replication of suitable natural biochemical signals, material surface properties, and material structure, remain the greatest challenges for the use of synthetic polymers for 3D tumor modeling.

More specifically, polyethylene glycol (PEG) based polymers have been used to some success as replacements for more natural biomaterials. Due to their high water content and mechanical properties, hydrated PEG gels closely resemble hydrogels assembled from naturally derived biomaterials, such as Matrigel. In addition, PEG polymers can serve as a "neutral template" of sorts, due to the possibility of adding novel biofunctional groups to the polymer, allowing for the manifestation of specific desired cell-environment interactions. So far, this approach has been used to graft various growth factors, such as bone-morphogenic protein-2 **[17]** and VEGF **[18]**, as well as to induce basic cell attachment via the grafting of fibronectin-derived RGDS peptide onto the surface of the polymer **[19]**.

Both natural and synthetic matrices provide their own specific suit of strengths and weaknesses, which are covered in more detail in *Table 1*. The greatest strength of naturally derived biomaterials is, as mentioned earlier, their natural biochemical and environmental properties. This makes them exceptionally suited for *in vitro* tumor modeling, as the natural milieu of tumor cells can be simulated far more easily and far more accurately than in synthetic models. While synthetic approaches, such as PEG-derived polymers, hold a significant degree of potential in terms of inducing specific cell-environment interactions. However, full replication of the large variety of biochemical signaling and biophysical properties found in *in vivo* tissues, still remains a distant dream for synthetic biomaterials. On the other hand, naturally derived biomaterials do possess significant downsides in certain key areas needed for 3D modeling. One of the key problems, associated with both collagen and Matrigel, is their relatively inflexible mechanical properties. While slight modifications using various methods, such as additional collagen crosslinking, can be performed to increase

hydrogel stiffness to a certain degree, the mechanical properties of naturally derived hydrogels generally cannot be significantly changed. This is due to the fact that changes to the matrix properties, via methods such as cross-linking and concentration increase, often result in altered biochemical profiles, which greatly complicates their use in 3D models **[16]**, especially for examining tumors that typically grow in stiffer environments, such as bones. In addition, cost still remains an important limiting factor in the use of natural biomaterials, as both purified type I collagen and Matrigel are relatively expensive, making their use in areas such as large-scale tumor screening, financially unviable. Synthetic polymers, on the other hand, are far cheaper, mechanically more malleable and tend to act in a far more predictable manner when compared to natural biomaterials.

Naturally derived matrices	
Examples of 3D Culture	Collagen, Matrigel (basement membrane), fibrin Permits 3D culture in physiological conditions with high viability
Bioactivity	Baseline bioactivity with ample ligands for cell adhesion and signalling Difficult to isolate the specific bioactive factor for experimental study Blocking antibodies to probe integrin effects (cell centered)
Mechanical properties	Tunable via additional crosslinking Generally alters ligand density Limited to low-range elasticities
Matrix degradation	Cell-mediated matrix remodeling Difficult to control
Growth factor contamination	Difficult to completely remove
Dynamic study	Generally short-term due to matrix remodeling
Advanced manipulations	Limited due to poor handling properties and non-specific bioactivity
Synthetic and semi synthetic matrices	
Examples of 3D Culture	PA, Polyesters, PEG PA: Toxic to 3D culture Polyesters: requires a processing step PEG- Full biocompatibility in 3D
Bioactivity	Requires passive protein adsorbtion (polyester) or extra engineering (PEG) Greater control over bioactivity with less experimental confounding Alter matrix design to probe integrin effects (cell extrinsic)
Mechanical properties	Tunable with minimal/no bioactivity change Broad range of physiological elasticities
Matrix degradation	Predictable degradation of synthetic material Requires modification for cell-mediated degradation
Growth factor contamination	None with synthetics
Dynamic study	Can be longer term
Advanced manipulations	Patterning and microfluidic techniques for complexity and controlled self culture

PA- polyacrylamide, PEG- Poly(ethylene glycol)

Table 1 – Benefits and disadvantages of synthetic and naturally derived 3-dimensional matrices. Table derived from West and Gill, 2014.

1.4 Aim of the project

Because of the corresponding suits of weaknesses and strengths found in both synthetic and natural biomaterials, the aim of this project was to determine if composite hydrogels, formed from PEG-based 'ABA' triblock copolymers and type I collagen, could be used for the three-dimensional modeling of liver tumors. We aimed to evaluate the composite hydrogels suitability for 3D tumor modeling based on three specific criteria. Firstly, based on the visual clarity of the composite hydrogel, a factor vital for continuous spheroid measurement and observation. Secondly, based on the rheological stiffness of the composite hydrogels, an aspect necessary for *in vitro* replication of both softer and stiffer tumor environments. Finally, we aimed to assess the actual growth of HepG2 spheroids when encapsulated within our composite hydrogels, both under normal conditions and when treated with anti-cancer agents. Contrasting these results to the control hydrogel, a 2.5% type I collagen hydrogel, it would be possible to evaluate the suitability of the PEG-based composite hydrogels when measured against more well-established 3D modeling approaches.

Our target polymers for such a model were all PEG-based 'ABA' triblock copolymers, the structure of which can be seen in *Figure 2*. We chose a PEG-based system for our composite hydrogel model due to their biocompatibility *in vitro* and *in vivo* **[20, 21]** and because, as mentioned earlier in Section 1.2, PEG-based hydrogel systems have been widely tested for potential 3D tumor modeling due to their inherently high biocompatibility and easily modifiable nature **[21,22]**. The key strength of cross-linked PEG-based 'ABA' triblock copolymers is their ease of use, as hydrogels can be formed simply by the addition of polymer into deionized H_2O and stirring. The formation of the

cross-linked hydrogel is catalyzed by A-A hydrophobic interactions between micelles, which causes the formation of physical cross-linking between the 'flower-like' micelles formed by the 'ABA' triblock copolymers **[23]**.

The polymers used for our composite polymer-collagen hydrogels could be largely divided into two larger families based on their side chain composition. All tested polymers either possessed benzyl side chains (Polymer 1) or vitamin E side chains (Polymers 2a, 2b, 2c, and 2d). Since variations of both benzyl and vitamin E containing triblock PEG polymers have been used by our lab in the past **[20, 23]**, we were confident that by using these variants, we could achieve a similar rheological profile displayed by normal collagen hydrogels. The reasoning behind the usage of either benzyl or vitamin E as the hydrophobic block A of the 'ABA' copolymer, is the fact that polycarbonates are synthesized by organocatalytic ring-opening polymerization which allows for control over the length of the A block and its functionalities. Furthermore, as vitamin E is more hydrophobic than benzyl, it explains the lower number of units needed for hydrogel formation. All these polymers have shown excellent biocompatibility in both human dermal fibroblasts and in mice and were therefore ideally suited for further cell cultivation studies **[23]**.

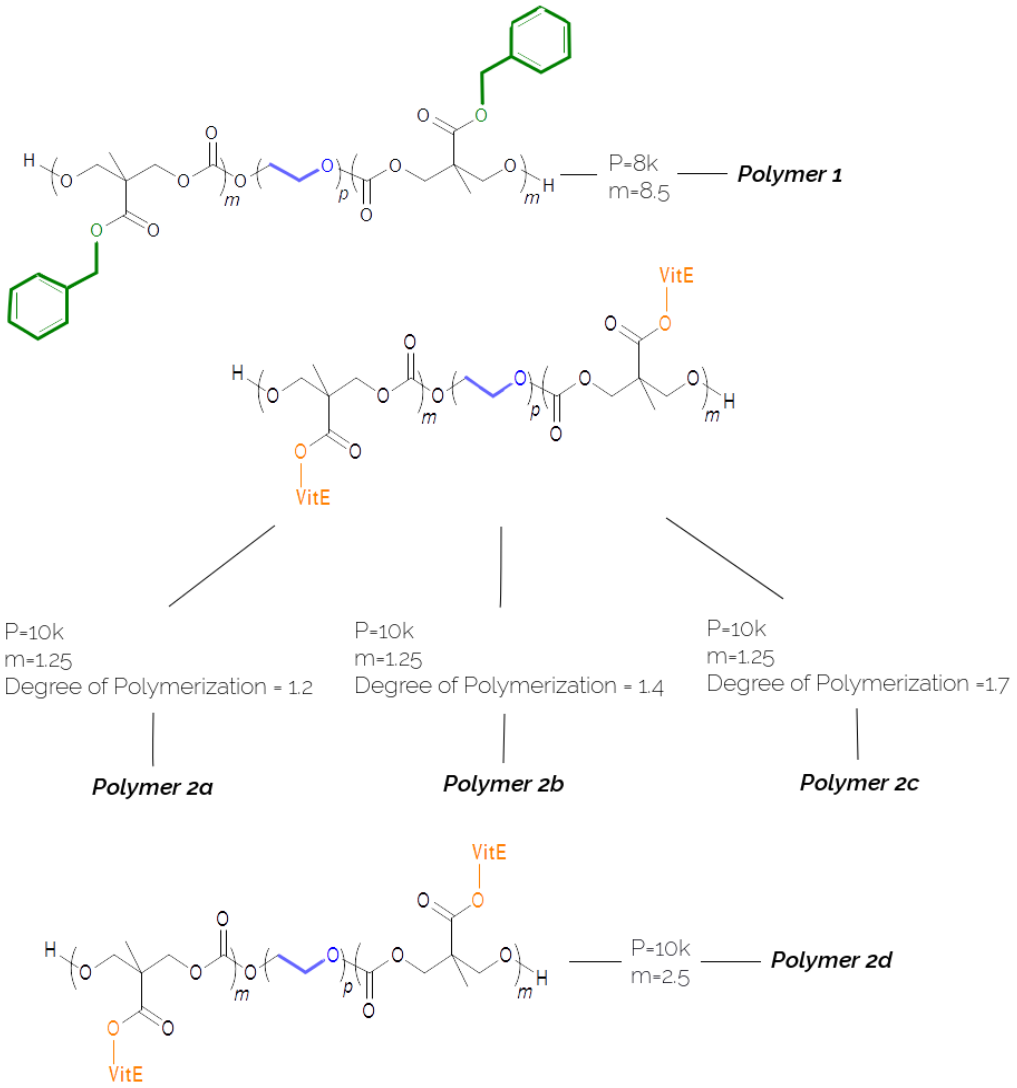

Figure 2 – PEG-based polymers for composite hydrogels. Chemical structures of Polymers 1, 2a, 2b, 2c and 2d used in composite hydrogel models. Three structural elements are indicated in separate colors: blue (PEG backbone), green (aromatic benzyl ring) and orange (Vitamin E subunit). P refers to the size of the PEG subunit while m refers to the number of repetitive units in the polymer side-chains. Degree of polymerization refers to the number of monomeric units in the polymer molecule.

2. Materials and Methods

2.1 Cell Culture

HepG2 liver cancer cell line, stored in liquid nitrogen, was used for cell culture (P<20). Cells were cultivated in Dulbecco's modified Eagle medium (with 4.5g glucose and L-glutamine), supplemented with 10% fetal bovine serum (FBS) and 1% penicillin. Cells were then subcultured for the duration of three days in a 37°C, 5% CO_2 incubator.

2.2 Agarose Plate Preparation

To induce cell aggregation and spheroid formation, HepG2 cells were cultivated on non-adhesive 96-well plates coated with agarose. A 1.5% agarose solution was formed by combining 300mL of 1x phosphate buffered saline (PBS) with 4.5g of agarose (1^{st} Base, Singapore). This mixture was then microwaved until the complete dissolution of the agarose into the solution could be observed. 75µl of heated agarose solution was then transferred to each well on the 96-well plates using a multi-headed pipette and allowed to cool for 30 minutes.

2.3 Spheroid Formation

Subcultured HepG2 cells were washed with 1x PBS and treated by 0.25% trypsin-EDTA for 5 minutes in a 37°C, 5% CO_2 incubator to facilitate cell detachment. Cells were then transferred to a 50ml falcon tube, followed by vortexing to physically break apart any remaining cell aggregates. Cell density in the resulting cell suspension was then measured using a C-Chip© disposable hemocytometer and HepG2 cells were seeded onto agarose covered 96-well plates at a cell density of 2000 cells per well. The 96-well plates were then subjected to 5 minutes of centrifugation at 1000rpm to facilitate the

formation of cell aggregates and then incubated for 3-4 days at 37°C, 5% CO_2, until the formation of spheroids.

2.4 **Collagen Gel Preparation**

Type I collagen (rat tail, 3mg/mL solution) was obtained from Life Technologies. A 2.5% collagen gel solution was formed using 10x PBS, 1N NaOH, and sterile distilled water, as per the manufacturer's instructions, which can be seen in *Figure 3*. The subsequent 2.5% collagen mixture was then stored on ice and 150µl of the solution was transferred into each sample well. HepG2 spheroids were then transferred from agarose-covered plates into the collagen-containing wells via pipette. Plates were then transferred to a 37°C, 5% CO_2 incubator for 45 minutes to allow the gel to solidify and 100µl of growth media (DMEM) was then added to each well and replenished daily.

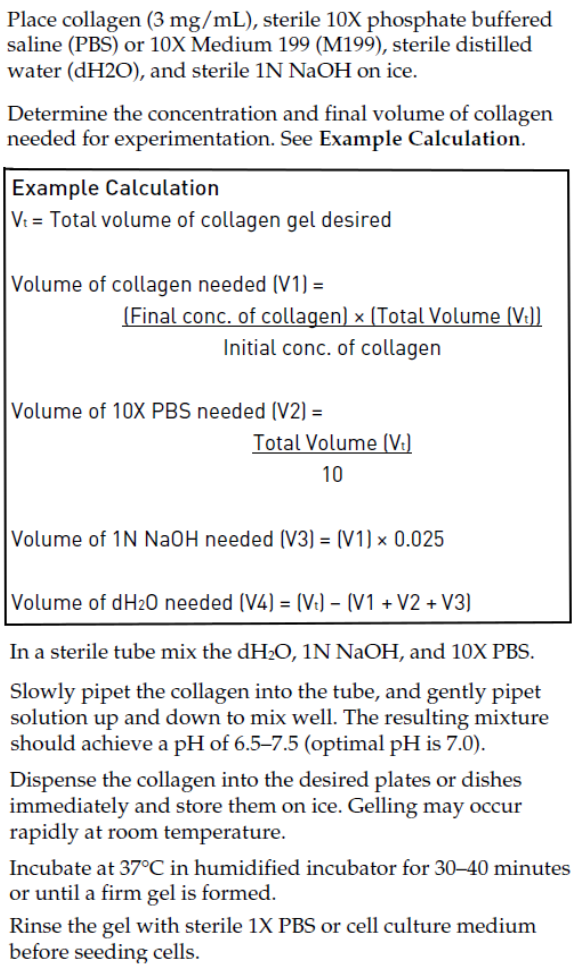

Place collagen (3 mg/mL), sterile 10X phosphate buffered saline (PBS) or 10X Medium 199 (M199), sterile distilled water (dH2O), and sterile 1N NaOH on ice.

Determine the concentration and final volume of collagen needed for experimentation. See **Example Calculation**.

Example Calculation

V_t = Total volume of collagen gel desired

Volume of collagen needed (V1) =

$$\frac{\text{(Final conc. of collagen)} \times \text{(Total Volume } (V_t))}{\text{Initial conc. of collagen}}$$

Volume of 10X PBS needed (V2) =

$$\frac{\text{Total Volume } (V_t)}{10}$$

Volume of 1N NaOH needed (V3) = (V1) × 0.025

Volume of dH_2O needed (V4) = (V_t) – (V1 + V2 + V3)

In a sterile tube mix the dH_2O, 1N NaOH, and 10X PBS.

Slowly pipet the collagen into the tube, and gently pipet solution up and down to mix well. The resulting mixture should achieve a pH of 6.5–7.5 (optimal pH is 7.0).

Dispense the collagen into the desired plates or dishes immediately and store them on ice. Gelling may occur rapidly at room temperature.

Incubate at 37°C in humidified incubator for 30–40 minutes or until a firm gel is formed.

Rinse the gel with sterile 1X PBS or cell culture medium before seeding cells.

Figure 3 – Guidelines for collagen hydrogel formation. Gelation instructions were provided by the manufacturer (Life Technologies).

2.5 Composite Gel Preparation

Both vitamin E and benzyl-based triblock copolymers were weighed for the desired concentration and dissolved in deionized water. The polymer solution was then transferred into wells on a 96-well plate and mixed with 2.5% collagen solution to achieve the final desired gel composition, with a total volume of 150µl per well. For vitamin E polymers with a degree of polymerization higher than 1.7, an additional heating step using an Eppendorf Thermomixer was performed at 60°C, 450rpm for 30

minutes, to achieve a homogeneous polymer solution. After formation of the composite solution, spheroids were transferred into the well via pipette and the gels were placed in an incubator at 37°C, 5% CO_2 for 45 minutes to facilitate gelation. DMEM was then subsequently added and replenished daily.

2.6 Spheroid Measurement

Spheroid diameters were observed and measured daily using a Leica DMI6000 B inverted light microscope at ten times magnification.

2.7 Rheological Measurement

Hydrogels were formed, using methods described in Sections 2.4 and 2.5, within 2.5ml Eppendorf tubes. The G'(Pa) of all tested hydrogels were then measured using an ARES G2 rheometer. Measurements were conducted using an 8mm parallel plate and under 0.7% strain.

2.8 Cell Viability Assay

Any remaining DMEM was removed from both the composite and collagen gel wells and 150µl of collagenase IV was added at 1mg/ml concentration. The plates were then returned to the 37°C, 5% CO_2 incubator for three hours, after which 27µl ($1/10^{th}$ of the volume present in each well) of PrestoBlue™ reagent was added to each well and incubated for a subsequent 18 hours. After incubation, absorbance was measured using a spectrometer at 570nm, using a 600nm reading as a reference wavelength for normalization.

2.9 Confocal Imaging

Collagen and composite gels were dissolved as outlined in section 2.7. Spheroids were then transferred into Lab-Tek Chambered Borosilicate Coverglass Trays and imaged using a confocal microscope.

3. Results

3.1 Visual Measurements

Over the course of 7 days, visual spheroid measurement in a variety of different composite hydrogels showed a large variability in spheroid response and growth rates between different gels. It became quickly obvious that composite hydrogels formed out of Polymer 1 showed an extremely high degree of opaqueness, making visual spheroid observations extremely difficult. However, Polymers 2a, 2b, 2c and 2d (*Figure 2*), formed a clearer hydrogel, although the degree of opaqueness present still surpassed that of the 2.5% collagen hydrogel, which was used as a control. The visual clarity of the variety of composite hydrogels can be seen in *Figure 4.* In addition, Polymer 1 hydrogels were shown to be difficult to dissolve, as both collagenase type IV and PBS were unable to dissolve the composite hydrogel. In comparison, for Polymers 2a, 2b, 2c and 2d, collagenase IV proved sufficient to dissolve the hydrogel for further studies.

Normal growth measurements of over the course of a week showed that the tested vitamin E composite gels fell into two separate categories (*Figure 5*). Lowest overall spheroid growth was shown in composite hydrogels formed using Polymer 2d. This low growth rate was observed at different concentrations, as a similar degree of reduced spheroid growth was seen at both 1.6mg and 3.3 mg concentrations. The second group of polymers, from the Polymer 2a/b/c family, showed better growth rates, closer to that observed in 2.5% collagen gels, especially Polymer 2c. When comparing between the growth rate of Polymers 2a, 2b and 2c, it seems that spheroid growth in composite hydrogels is somewhat dependent on the degree of polymerization (DP) possessed by

the polymers, as increasing the DP from 1.2 to 1.7 (from Polymer 2a to 2c) resulted in a noticeable increase in both spheroid size and volume. Due to the high degree of structural similarity between Polymer 2a/2b/2c and the Polymer 2d, the lowered growth rate is most likely due to the increased amount of vitamin E side-chains in Polymer 2d, changing the mechanical and micro-environmental structure of the composite hydrogel. In addition, a high degree of variability is visible in the data. This is most likely due to the inherent batch to batch variability between spheroid cultivation cycles, spheroid cell counts, size and, most importantly, spheroid cohesion - all of which can vary by quite a fair margin from batch to batch. It is quite likely that due to lowered spheroid cohesion in the spheroid cultivation batch, the transfer process may have caused the outer periphery of cells shear off during the transfer process, and through that, increased the degree of variation present in the dataset. Nevertheless, the two categories mentioned earlier were still clearly distinguishable, even with increased variability present in the data.

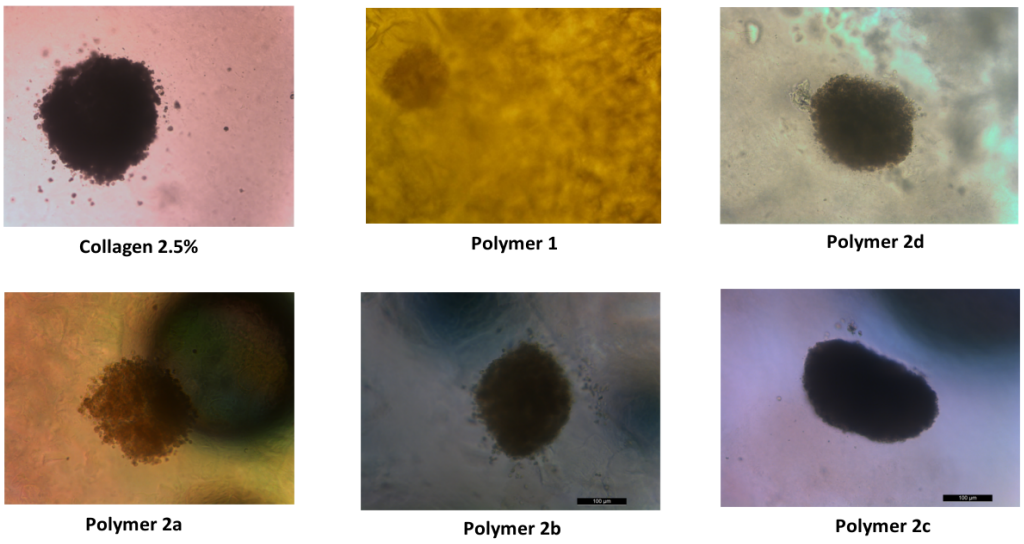

Figure 4 – Visual clarity of composite hydrogels. All composite hydrogels were formed using 1.66% collagen concentration and images shown above were taken on Day 1.

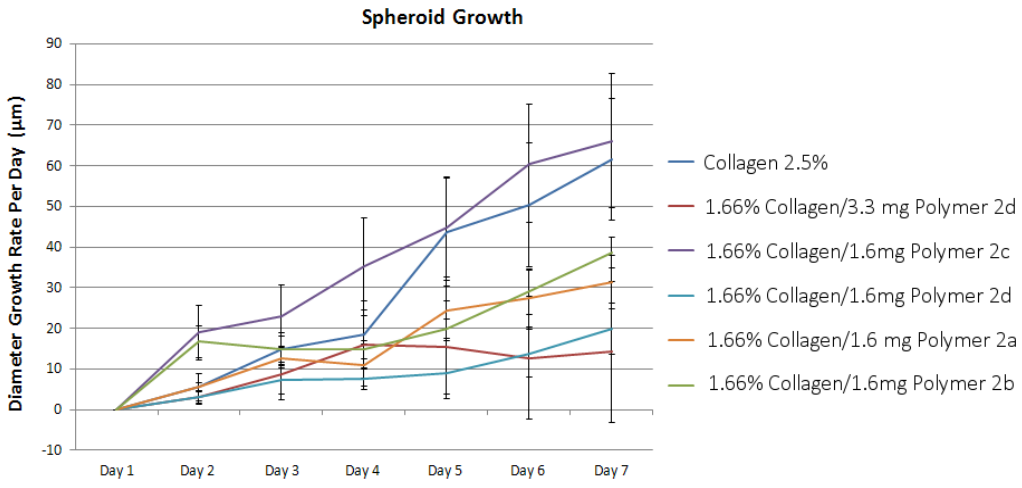

Figure 5 – Hydrogel encapsulated spheroid growth over seven days. Measurements of the average spheroid diameter increase, in micrometers, over the course of seven days. Spheroid size at Day 1 was considered to be the zero value. Error bars represent the standard error of the provided values.

When doxorubicin (Dox) was added to hydrogel encapsulated HepG2 spheroids, the encapsulated spheroids showed much lower levels of doxorubicin response when compared to normal, unencapsulated, spheroids (*Figure 6*). Even when treated with doxorubicin, a DP-associated increase in spheroid growth was observed between the composite hydrogels, as an increase in the degree of polymerization of the polymer was observed to result in higher growth and lowered doxorubicin response. Furthermore, Polymer 2c composite hydrogels showed growth rates surpassing even that of normal 2.5% collagen gels. This trend was further confirmed when the doxorubicin concentration was increased by five times (*Figure 7*), where a similar decrease in doxorubicin response could be observed between the 2c variant and the 2.5% collagen hydrogel. We then treated the spheroids using our in-lab experimental doxorubicin carrier system, which implements boronic acid/urea based mixed micelles to load and

carry doxorubicin. This system, formed using acid-functionalized and urea-functionalized diblock copolymers, has shown high levels of drug loading in our in-lab tests, as well as showing a pH-dependent release of doxorubicin *in vitro*. However, tests using doxorubicin loading mixed micelles further reinforced the data obtained using free doxorubicin, as drug resistance in the 2c composite hydrogels was still seemingly higher than in comparative collagen hydrogels.

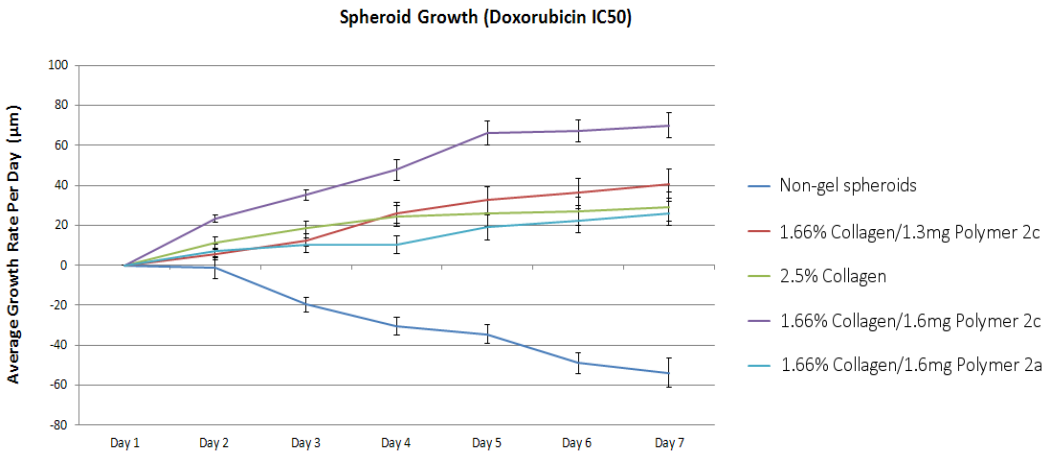

Figure 6 – Spheroid Growth after Doxorubicin Treatment (IC50). Measurements of the average spheroid diameter increase, in micrometers, over the course of seven days after doxorubicin treatment. Spheroid size at Day 1 was considered to be the zero value. Error bars represent the standard error of the provided values.

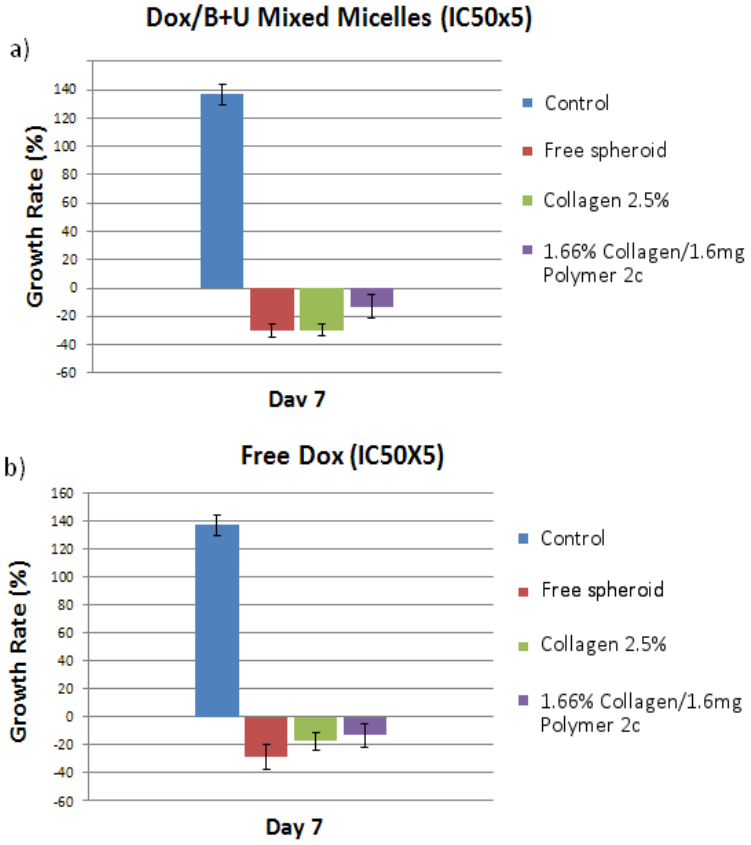

Figure 7 – Spheroid growth rate at day 7 after doxorubicin treatment (IC50x5). Spheroid volume increase or decrease compared to the day 1 values. Control refers to non-encapsulated media suspended spheroids, without doxorubicin treatment. Free spheroid refers to non-encapsulated media suspended spheroids, with doxorubicin treatment (at IC50x5). Free Dox (b) refers to results obtained from using free doxorubicin, while Dox/B+U Mixed Micelles (a), refers to results obtained using our in-lab doxorubicin/boronic-urea based mixed micelle system.

3.2 Rheological Measurements

Rheological measurements regarding the stiffness of the various hydrogels in question have been summarized in *Figure 8*. From the results, we can see that Polymer 1 composite hydrogels showed a far higher G'(Pa) value at 1Hz than the 2.5% collagen hydrogel used as a control. However, vitamin E based triblock copolymers all showed a stiffness profile far more similar to that of the 2.5% collagen control (136 G'(Pa)). In

terms of individual G'(Pa) values, a stepwise increase in hydrogel stiffness was found to correspond to an increase in the degree of polymerization within the Polymer 2a/b/c family. Polymer 2a composite hydrogels were shown to be around 85 G'(Pa), while Polymer 2b and 2c variants showed a G'(Pa) value 145 and 214, respectively.

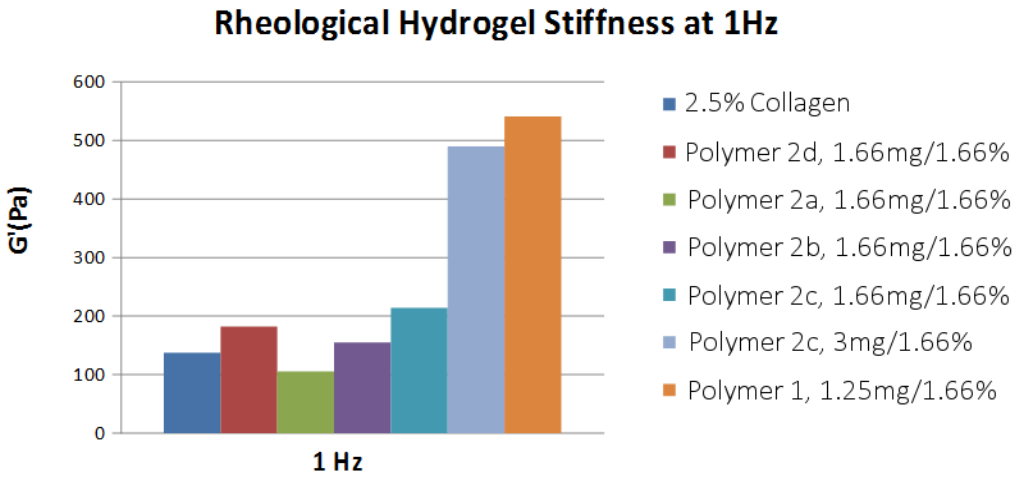

Figure 8 – Rheological stiffness of composite hydrogels at 1Hz. G'(Pa) refers to the storage modulus value at 1Hz. One 1Hz is equivalent to the Angular Frequency at 6.3 rad/s. Percentage values in the legend refer to the concentration of collagen present in the composite hydrogels.

Hydrogel Composition	G'(Pa) at 1Hz
2.5% Collagen	137
Polymer 2d 1.66mg/1.66%	182
Polymer 2a, 1.66mg/1.66%	105
Polymer 2b, 1.66mg/1.66%	155
Polymer 2c, 1.66mg/1.66%	214
Polymer 2c 3.3mg/1.66%	490
Polymer 1, 1.25mg/1.66%	541

Table 2 – Rheological stiffness of composite hydrogels at 1Hz. G'(Pa) refers to the storage modulus value at 1Hz. One 1Hz is equivalent to the angular frequency at 6.3 rad/s. Percentage values refer to the concentration of collagen present in the composite hydrogels.

3.3 Confocal Imaging

Summarized in *Figure 9*, confocal imaging results of spheroids treated with free doxorubicin and boronic-urea based doxorubicin micelles at five times the IC50 value, showed a significant level of doxorubicin uptake (for both free doxorubicin and the micellar form) within the spheroids. However, while high levels of drug uptake were seen in non-encapsulated spheroids, spheroids grown in 2.5% collagen and spheroids obtained from Polymer 2b composite hydrogels, visible drug permeability in the Polymer 2c composite hydrogels was greatly reduced in comparison to the other samples. In addition, the boronic-urea based doxorubicin micelle system seemingly showed a slightly higher degree of drug accumulation within the HepG2 spheroids when compared to the free doxorubicin treatment. However, the degree of increased brightness observed was quite slight, necessitating the use of further, more quantifiable, studies to accurately determine the effectiveness of the Dox/B+U micelles when compared to free doxorubicin.

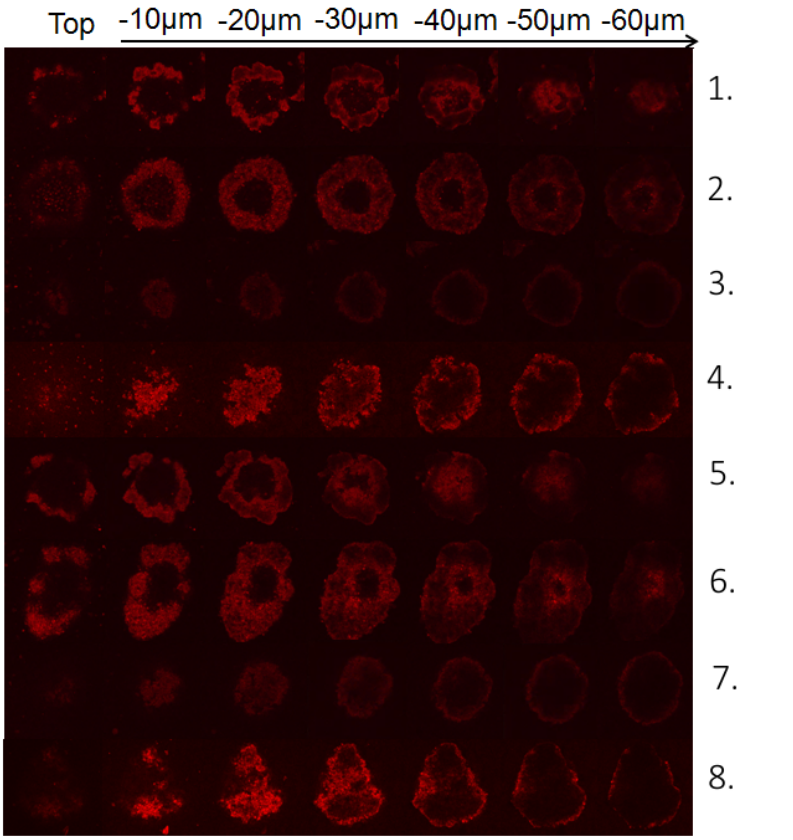

1) 2.5% Collagen spheroid (Free Dox IC50 X5)

2) Non-gel HepG2 spheroid (Free Dox IC50 X5)

3) Polymer 2c 1.6mg/1.66% (Free Dox IC50 X5)

4) Polymer 2b 1.6mg/1.66% (Free Dox IC50 X5)

5) 2.5% Collagen spheroid (Dox Micelle IC50 X5)

6) Non-gel HepG2 spheroid (Dox Micelle IC50 X5)

7) Polymer 2c, 1.6mg/1.66% (Dox Micelle IC50 X5)

8) Polymer 2b, 1.6mg/1.66% (Dox Micelle IC50 X5)

Figure 9 – Confocal imaging of hydrogel encapsulated HepG2 spheroids. Distribution of doxorubicin within the spheroids has been visualized by red coloring. Imaging starts from the first sign of fluorescence (Top) and subsequent images were taken after every 10 micrometers. Percentages in the naming scheme refer to the percentage of collagen present in the composite hydrogels. All images have been brightened by 50%.

3.4 Cell Viability Assay

A comparison cell viability assay between the Polymer 2b and 2c composite hydrogels, and the collagen control was set up using PrestoBlue™ reagent, the results of which can be seen in *Figure 10.* Overall cell viability amongst the hydrogels was of a relatively similar level, with Polymer 2c composite hydrogels showing slightly higher levels of absorbance and with the 2.5% collagen hydrogels and the Polymer 2b composite hydrogels showing slightly smaller amounts of cell viability. The lowest amount of cell viability was, however, clearly shown by the standard two-dimensional cell culture model. However, while all composite gels showed a higher degree of cell viability when compared to the equivalent 2D model, a further, larger scale cell viability study is necessary to better establish the differences between the various hydrogels when it comes to cell viability.

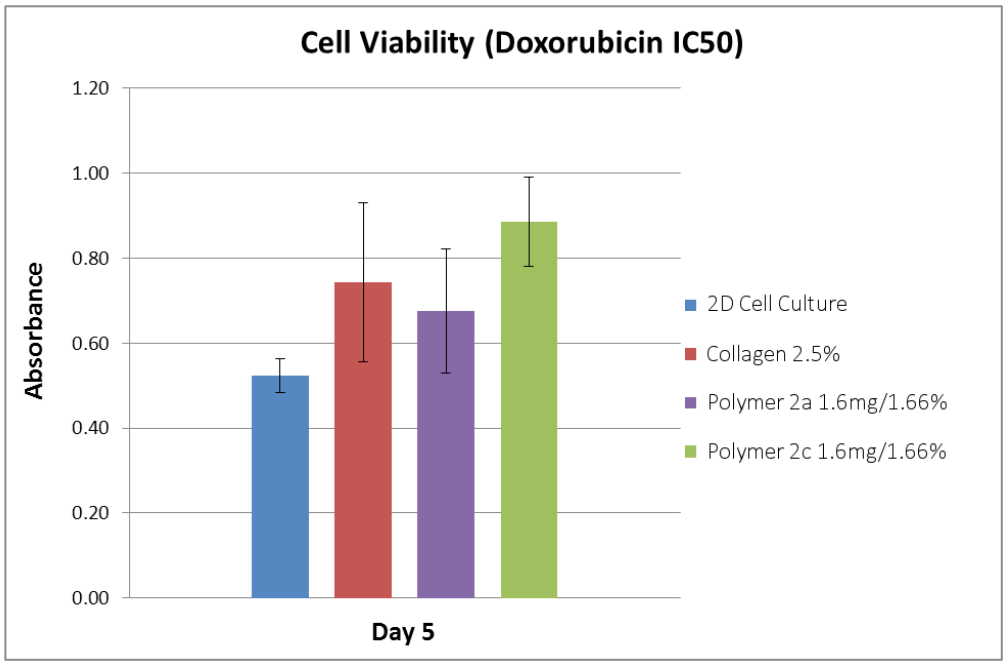

Figure 10 – Cell viability comparison of composite hydrogels under doxorubicin conditions. Percentages in the naming scheme refer to the percentage of collagen present in the composite hydrogels. 2D cell culture refers to standard attachment culture seeded and cultivated at the equivalent level to the hydrogels in identical environments (2000 cells for 5 days, 96-well plate).

4. Discussion

4.1 Composite hydrogel environment

Changes in the overall hydrogel environment have been shown to possess a significant effect on a variety of different tumor cell parameters. Most important amongst these environmental factors is hydrogel stiffness, which has been shown to be responsible for a variety of different tumor cell characteristics, such as invasion and metastasis **[24]**, as well as overall bioactivity and drug resistance **[16]**.

Hydrogel stiffness is also one of the major weaknesses associated with natural biomaterials. Because of the naturally low G'Pa that collagen hydrogels exhibit, their use as 3D models is currently only limited to tumors occurring in softer tissue (such as the liver) and not to cancers occurring in stiffer environments (such as bone). While the stiffness of collagen hydrogels can be increased via chemical methods such as collagen cross-linking, such approaches have been shown to have their own significant downsides, as they result in altered matrix biochemistry, complicating further studies **[25]**.

The overall stiffness profile of our tested composite hydrogels varied significantly, due to a variety of factors, such as concentration, degree of polymerization and feed ratio, but most importantly due to structural differences between the polymers. The largest and most visible difference in terms of hydrogel stiffness could be seen between the benzyl-based composite hydrogels and the other tested hydrogels. While higher levels hydrogel stiffness were achieved in composite gels using this polymer, we were unable to replicate the naturally softer G'(Pa) values traditionally associated with collagen

hydrogels (in our case, our 2.5% collagen hydrogel control). This could be due to a number of reasons, but one possible explanation could be due to the increased amount of pi-stacking taking place between aromatic benzyl rings present in the side-chains of the Polymer 1, which would increase non-covalent interactions between the rings and result in increased hydrogel stiffness.

On the other hand, hydrogels formed using vitamin E based triblock copolymers (and its variants), displayed a stiffness profile far closer to that of our collagen control. In addition, vitamin E based hydrogels still showed a remarkable level of modularity in terms of stiffness, as an increase in the overall G'Pa could be seen with the increase in both the concentration and the degree of polymerization present in the polymer. More specifically, Polymers 2a, 2b, and 2c showed the most similar results to that of the 2.5% collagen control. Additionally, changes to the degree of polymerization, allowed for relatively precise manipulation (in the area of 60-70 G'Pa) of composite hydrogel stiffness. An increase in the concentration of the polymer, however, resulted in a corresponding, larger, increase in hydrogel stiffness, up to the 500 G'Pa range. All this indicates that when used in a composite hydrogel, the 2a/b/c family of polymers can not only replicate the natural level of stiffness found in normal collagen hydrogels but can also potentially greatly elevate rheological hardness of the composite hydrogel, suggesting that the mechanical parameters of the tested vitamin E composite hydrogels are highly malleable and easily modifiable.

4.2 Visual observations and spheroid growth

Visual observation of spheroid diameter has often been used in 3D tumor models as a representation of tumor growth and this has been used to assess the potential viability

of 3D models in both liver **[12]** and breast cancer **[26]**. The transparent nature of naturally derived hydrogels serves as a great boon in this, as observations can be performed over a longer period without actually dissolving gel matrix. It is because of this that the transparency of our proposed composite system is of paramount importance. If visible measurements cannot be performed, the potential usability of our proposed system diminishes significantly.

It is in this that we faced the largest problems associated with our composite hydrogel systems. In general, the PEG-based polymers that were used all resulted in the loss of a certain degree of transparency when compared with the collagen control. The transparency of the various hydrogels can be better seen in *Figure 4*. The most visibly opaque hydrogels were formed by the Polymer 1 composite hydrogels while the vitamin E based composite matrices showed a smaller, but still noticeable, increase in hydrogel opaqueness. For vitamin E based hydrogels, we found that spheroid placement inside the gel suddenly became much more vital for accurate spheroid measurement. More specifically, spheroids placed nearer to the bottom of the well were far more visible than spheroids placed in the upper half of the hydrogel (*Figure 11*). By specifically transferring the spheroids to the lower third of the hydrogel (as opposed to simply transferring them into the gel without concern for their position within it), we were capable of increasing the quality of our visual measurements to an acceptable range. However, even using this method, we were not capable of actually achieving good visual clarity for spheroids cultivated in Polymer 1-based hydrogels.

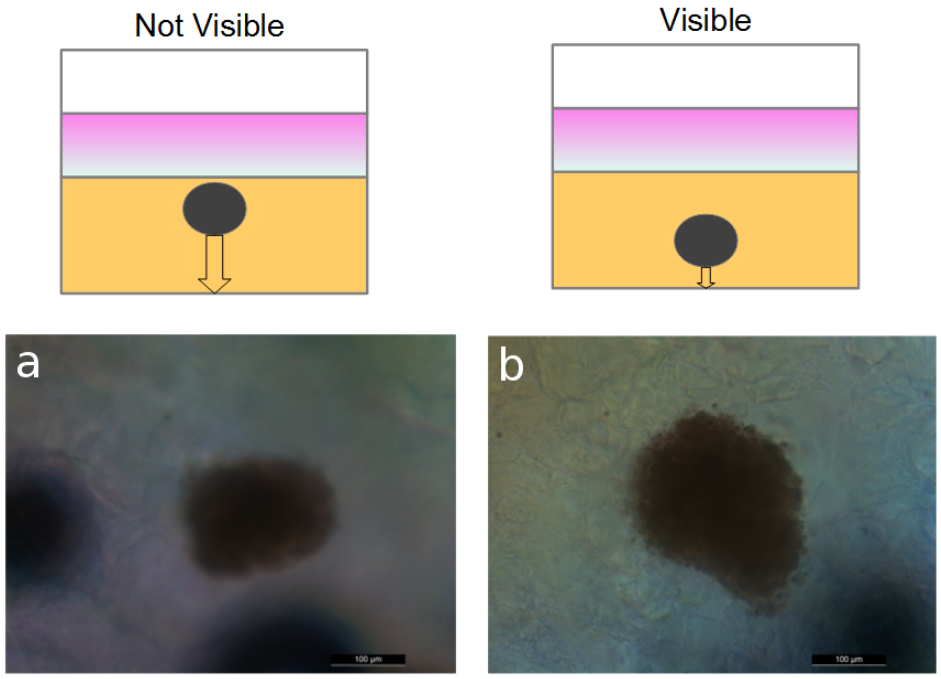

Figure 11 – The effect of spheroid localization on visibility. Contents of hydrogel wells have been represented in four colors: yellow (hydrogel), pink (DMEM media), white (empty well space) and black (HepG2 spheroid). The arrow represents the approximate position of the spheroids in regards to the bottom of the 96-well. From the two images, one represents a spheroid with blurred boundaries (a) and the other represents a spheroid with clear boundaries (b). Blurriness increases proportionally with distance from the bottom of the well. Scale bar represents the distance of 100 micrometers.

As mentioned in Section 3.1, visual diameter measurements of encapsulated spheroids showed a high amount of variability in their growth rate. The lowest amounts of growth were observed in spheroids encapsulated in Polymer 2d composite hydrogels. The amount of growth shown in these hydrogels (approximately 20µm by Day 7) was far below that shown by the collagen control (approximately 50µm by Day 7). A similar pattern of growth was also seen in higher concentration variants of the composite hydrogel in question, suggesting that it was an intrinsic property of the polymer in question, rather than an effect caused by increased stiffness or concentration. Because of the structural similarities between other members of the Polymer 2 family, this is

most likely due to increased amount of hydrophobicity caused by the higher number of hydrophobic vitamin E groups attached to the PEG backbone. Another potential reason could be hydrogel porosity, as the increased number of side-chains may lead to the formation of smaller pores in the Polymer 2d composite hydrogel itself, thereby negatively affecting spheroid growth.

Polymer 2a/b/c family hydrogels, however, showed higher rates of growth, more closely mimicking spheroids grown in the 2.5% collagen hydrogel. In particular, the Polymer 2c showed extremely similar growth rates (approximately 45 μm by Day 7) to the control. In general, variations in the degree of polymerization resulted in a significant difference in spheroid size, as can be seen from the lower spheroid growth rates shown by the Polymer 2a and 2b composite hydrogels. All in all, using the 2c variant of the vitamin E polymer, we were capable of replicating results shown by hydrogels formed from natural biomaterials, indicating that our composite polymer-collagen hydrogel can be used as a substitute for pure collagen hydrogels, without causing a negative impact on the growth rate of liver tumor cells.

4.3 Response to anti-cancer treatment

To further examine the effects of the composite hydrogel on the encapsulated spheroids, we conducted a series of growth experiments using doxorubicin. Doxorubicin is a chemotherapeutic antitumor agent that is in wide-scale medical use for treating a variety of different carcinomas and sarcomas in cancer patients. In research, doxorubicin is used mainly due to its ease of use and natural photosensitivity. It is often among the first drugs to be tested in novel tumor models and has been in use in patients for over three decades **[27]**

An initial doxorubicin study, conducted over the course of seven days (doxorubicin added at the IC50 value), showed surprising results. Out of all the hydrogels tested, the highest doxorubicin resistance was shown by spheroids cultivated in Polymer 2c hydrogels, even surpassing the results displayed by the 2.5% collagen control. Even at a lower polymer concentration, Polymer 2c composite hydrogels still showed equivalent results to the collagen baseline and displayed equivalent amounts of spheroid growth. As shown by previous studies **[12, 16],** non-encapsulated spheroids display a much lower degree of doxorubicin resistance when compared to spheroids encapsulated in hydrogels, something which we also observed from our data, where non-encapsulated spheroids showed a markedly lower degree of doxorubicin resistance in comparison to our tested hydrogels. While Polymer 2a composite hydrogels displayed a lower growth rate compared to the Polymer 2c hydrogels, the level of growth displayed was still equivalent to the 2.5% collagen hydrogel control, achieving similar results.

A more limited secondary study with increased doxorubicin amounts (IC50x5) was also carried out. Experimental results obtained from this secondary study further corroborated the original data (*Figure 7*), as even at far higher concentrations, Polymer 2c hydrogels consistently showed a lowered response to doxorubicin in comparison to both the collagen hydrogels and non-encapsulated spheroids. This data was further reinforced by replicate studies done using our experimental Dox/B+U mixed micelle system, in which Polymer 2c composite hydrogels yet again showed similar levels of increased drug resistance in comparison to the 2.5% collagen hydrogel and the non-encapsulated spheroid control. A similar result could be seen from the PrestoBlue® testing, where Polymer 2c composite hydrogels showed slightly higher levels of overall

cell viability under doxorubicin (IC50) conditions when compared to either the collagen control or the Polymer 2b composite hydrogel, as can be seen from *Figure 10.*

From our perspective, there were two potential explanations for this sudden, and quite dramatic, increase in doxorubicin resistance. Firstly, this could be a natural cellular response triggered by the altered cellular environment present in the composite hydrogels. While the gross mechanical strength of the Polymer 2c composite hydrogels was quite similar to those displayed by the 2.5% collagen control (*Figure 8*), even microenvironmental changes in synthetic polymer networks can result in significant changes in cell organization and dissemination **[28]**. Secondly, and more likely, the reason for this increased doxorubicin resistance was due to lowered drug permeability through the hydrogel, which would result in lower levels of doxorubicin reaching the cells. To see whether or not this was the case, we conducted confocal microscopy study, taking advantage of the natural photosensitivity of doxorubicin to display the amount doxorubicin reaching the HepG2 cells, which would allow us to determine whether or not drug permeability was causing the lowered anti-cancer response.

Confocal imaging results can be seen in *Figure 9* and show a generally high uptake of doxorubicin in most of the spheroids cultivated in composite hydrogels. The only exception for this is the Polymer 2c composite hydrogel, where lower overall uptake for both the free and micellar boronic-urea form of the doxorubicin, was observed. This lack of drug uptake, at least to the same degree, was not observed in Polymer 2b-based composite hydrogels, suggesting that the increase in the degree of polymerization of the polymer was at least partially responsible for lowered doxorubicin penetration through the composite hydrogel. This aspect is most likely also responsible for the increased

doxorubicin resistance observed in visual testing. The results obtained are rather troubling, as they seem to suggest that the polymers within composite hydrogels may actively hinder the entry of various anti-cancer drugs, at the very least the entry of doxorubicin, potentially calling into question their use as a relevant platform for anti-cancer drug testing. Further studies using anti-tumor agents with varying chemical properties and structures are needed to look into this aspect in depth, as doxorubicin may, in actuality, be binding to the polymer portion of the composite hydrogel. This may be happening through several potential mechanisms. For example, there might be hydrophobic interactions between the vitamin E group and the hydrophobic groups present on doxorubicin. Another potential cause for this may be hydrogen bonding between the PEG group and the peripheral -OH and O groups present on doxorubicin. However, while the Polymer 2c composite hydrogel is not, in actuality, increasing the rates of doxorubicin resistance, the high cell growth observed in these hydrogel models does still indicate that an equal rate of spheroid growth to that of the 2.5% collagen control can be achieved in Polymer 2c composite hydrogels, despite the lowered levels of doxorubicin permeability.

5. Conclusion

Five polyethylene glycol-based polymers were synthesized and tested for their potential suitability for a composite polymer-collagen hydrogel model for three-dimensional tumor modeling. A variety of key factors vital for 3D tumor models, such as hydrogel stiffness, visibility, and cell growth were observed, and the results were compared to a 2.5% collagen hydrogel, used as a control.

Firstly, the transparency of the composite hydrogels was assessed. As transparency of hydrogels is vital for observing spheroid growth and response in real time, a sufficient degree of transparency in tested composite hydrogels was extremely important **[29]**. Overall, the transparency of composite hydrogels was lower than that of the collagen control. Polymer 1 showed exceptionally low visibility, to the point where in the vast majority of the cases the spheroids were completely unidentifiable using a light microscope. For Polymers 2a, 2b, 2c, and 2d, visibility was lower when compared to the collagen control, but still sufficient for proper measurement and observation. In addition, clarity in Polymers 2a, 2b, 2c, and 2d, could be further increased via the careful placement of the spheroid in the lower third of the hydrogel.

Secondly, the stiffness of composite hydrogels was measured using a rheometer. Results showed that even at the lowest possible polymer concentrations, Polymer 1 showed the highest level of mechanical stiffness, approximately five times that of the 2.5% collagen hydrogel while Polymer 2b composite hydrogel showed a stiffness profile closest to that of the collagen control. In general, Polymers 2a, 2b, 2c, and 2d were found to have a relatively similar stiffness range to that of the 2.5% collagen hydrogel while displaying a

minor stepwise increase in G'(Pa) corresponding to the increasing degree of polymerization. In addition, Polymer 2c stiffness was shown to be responsive to polymer concentration increase, which greatly increased the G'(Pa) of the composite hydrogel, showing a high degree of mechanical malleability. At this point, due to the inherent opaqueness of the hydrogel and its extremely high stiffness, we decided to set aside Polymer 1 composite hydrogels and focus our attention on Polymer 2-family composite hydrogels for further testing.

When measuring tumor spheroid size, Polymer 2c showed the closest growth rates to that of the control, while both Polymer 2a and 2b composite hydrogels showed overall lower spheroid growth. Lowest amount of cell growth was displayed by Polymer 2d composite hydrogels, where extremely low rates of growth (~20μm) were seen at comparable polymer/collagen concentrations to other tested hydrogels. Similar results were also seen when the polymer concentration was doubled. As with Polymer 1, we set aside Polymer 2d for our further studies, as the composite hydrogel environment was shown to be unsuitable tumor cell cultivation. Growth observations under normal conditions were then followed up by the examining spheroid response to anti-cancer drugs, namely doxorubicin.

Doxorubicin testing showed that Polymer 2c composite hydrogels showed unusually low levels of doxorubicin response, both at lower and higher drug concentrations. Other composite hydrogels (Polymers 2a and 2b) showed approximately equivalent growth rates to the control. Similar results, showing higher levels of doxorubicin resistance in Polymer 2c composite hydrogels, were also obtained from cell viability assays. Further studies using confocal microscopy showed that the Polymer 2c composite hydrogels

suffer from lowered permeability, reducing the levels of doxorubicin reaching the HepG2 spheroids. This suggests that a relatively minor change in the degree of polymerization can have significant effects on drug penetration in composite hydrogels.

All in all, several considerable difficulties remain with the complete application of composite hydrogels as a three-dimensional tumor model. Even though we were capable of generating a number of composite hydrogels (members of the 2a/b/c family) that showed a relatively high degree of cell growth, while possessing stiffness profile similar to that of collagen hydrogels, and one polymer (Polymer 2c) in particular was capable of showing almost identical levels of spheroid growth to those found in our collagen control, problems such as low drug permeability, reduced cell growth and visibility still remain key issues to overcome in all our tested composite hydrogels. Most importantly, the largest issue currently limiting the usage of composite hydrogels as a tumor model is their relative unwieldiness. This is due to the fact that one of the key issues restricting the usage of biologically derived hydrogels, in addition to their price, is the relatively high amount of expertise needed to conduct various assays using materials such as type I collagen and Matrigel. In this aspect, a lot of work is needed to further refine our composite hydrogels from a usability standpoint, as several additional steps (such as heating) were added to facilitate the proper formation of our composite hydrogels.

Nevertheless, if current difficulties could be overcome, potential still remains for the use of composite hydrogels 3D tumor modeling, as we were capable of producing a hydrogel that closely mimicked the standard collagen hydrogel in terms of rheological stiffness and cell growth. Since the characteristics of composite hydrogels can be greatly changed

via the use of various side-chains, degrees of polymerization and both the polymer and collagen concentrations, it is quite likely that by varying these parameters, it is possible to overcome the problems currently associated with the tested composite hydrogels.

6. Future work

From our studies, we have identified Polymer 2c as the most suitable target for use in a composite three-dimensional hydrogel model. Further optimization studies involving larger variety of polymer and collagen concentrations, different tumor cell lines (such as MDA-MB-231 breast cancer cells), use of different anti-cancer drugs and a more in-depth study of the mechanical properties and the overall structure of the composite hydrogels would allow for a more thorough characterization and optimization of our proposed tumor model. Due to their quite similar structure, further studies using the other members of Polymer 2a/b/c family may also provide further insight into Polymer 2c, especially in terms of structural factors such as permeability (as that has been shown to differ between the polymers in question) and porosity. Spheroid growth studies could be expanded on as well, using methods such as fluorescence activated cell sorting (FACS) to count the specific number of cells in each spheroid before and after treatment, along with further replicate studies involving normal, non-treated, HepG2 spheroid growth in composite hydrogels to reduce the variation present in the current dataset.

When discussing specific permeability studies, further research using more or less hydrophobic and reactive anti-cancer drugs could be used to determine whether or not the reduced doxorubicin permeability is due to binding to the polymer present in the composite hydrogels. Studies including more hydrophobic anti-tumor agents (such as Paclitaxel) as well as more non-reactive agents (a non-hydrophobic control molecule with a marker), could potentially allow for a far better understanding of the topic.

In addition, up-regulation of various growth and pro-angiogenic factors, such as HIFα and VEGF-A has also been shown to be an important key difference between 2D and 3D tumor models **[30]**. Quantitative reverse transcription polymerase chain reaction (qRT-PCR) studies could potentially shed light on whether or not polymer-collagen composite hydrogels show an equivalent level of increased gene expression when compared to fully collagen-based hydrogels. Efforts towards perfecting the usability of the composite hydrogel model should also be increased. This is due to the fact that currently, the composite hydrogel model is relatively unwieldy and requires a high amount of experience and practice for its normal use. This is mainly caused by the viscous nature of the dissolved 2c polymer (at the tested concentrations), which requires an additional heating step to allow the polymer solution to be transferred via pipette. In addition, further complications arise from the spheroid transfer process itself, as well as from the limitations on spheroid location within the hydrogel, which is imposed by the opaque nature of the composite hydrogels tested. Both of these problems could be potentially reduced (or even removed entirely) by proper concentration optimization or possibly via minor chemical alterations to the Polymer 2 itself.

Finally, further research could also be carried out to assess the viability of composite hydrogels as a subcutaneous tumor carrier for xenografts in animal models. While Matrigel is typically used for tumor inoculation, recent studies have shown, that for of certain types tumors, such as ovarian tumors, tumor cells inoculated from collagen hydrogels show a higher degree of vascularization when compared to cells grown in Matrigel, alginate or agarose **[31]**. Due to similar tumor cell growth rates displayed by the Polymer 2c composite hydrogels, it is possible that a similar rate of *in vivo* may also

be achievable using composite hydrogels, greatly increasing the cost viability and accessibility of various tumor modeling studies.

References

1. American Cancer Society, *Global Cancer Facts and Figures 3rd Edition,* 2011. p. 1-10

2. Holohan, C., et al., *Cancer drug resistance: an evolving paradigm*. Nature Reviews: Cancer, 2013. **13**(10): 714-26

3. Bixby, D., Talpaz, M., *Seeking the causes and solutions to imatinib-resistance in chronic myeloid leukemia*. Leukemia, 2011. **25**(1): 7-22

4. Wang, C., et al., *Three-dimensional in vitro cancer models: a short review.* Biofabrication. 2014. **6**(2): 022001

5. Ridky, T.W., et al., *Invasive 3-Dimensional Organotypic Neoplasia from Multiple Normal Human Epithelia.* Nature Medicine, 2010. **16**(12):1450-5

6. Kelland, L.R., *Of mice and men: values and liabilities of the athymic nude mouse model in anticancer drug development.* European Journal of Cancer, 2004. **40**(6):827-36.

7. Hayes, S.A., et al., *From mice to men: GEMMs as trial patients for new NSCLC therapies.* Seminars in cell and developmental biology, 2014. 27:118-27

8. Sutherland, R.M., *Cell and environment interactions in tumor microregions: the multicell spheroid model.* Science, 1988., **240**(4849):177-84

9. Desoize, B., Jardiller, J., *Multicellular resistance: a paradigm for clinical resistance?* Clinical Reviews in Oncology/Hematology, 2000. **36**(2-3):193-207

10. Friedrich, J., et al., *Spheroid-based drug screen: considerations and practical approach.* Nature Protocols, 2009. **4**(3):309-24

11. Yamada, K.M., Cuikerman, E.*, Modeling Tissue Morphogenesis and Cancer in 3D.* Cell, 2007. **130**(4):601-10

12. Yip. D., et al., *A multicellular 3D heterospheroid model of liver tumor and stromal cells in collagen gel for anti-cancer drug testing*. Biochemical and Biophysical Research Communications, 2013. **433**(3):327-32

13. Weaver, W.M., et al., *β4 integrin-dependent formation of polarized three-dimensional architecture confers resistance to apoptosis in normal and malignant mammary epithelium*. Cancer Cell, 2002. **2**(3):205-16

14. Yang, Y., et al., *The Notch ligand Jagged2 promotes lung adenocarcinoma metastasis through a miR-200–dependent pathway in mice*. Journal of Clinical Investigation, 2011. **121**(4):1373-85

15. DelNero, P., et al., *Microengineered tumor models: Insights & opportunities from a physical sciences-oncology perspective*. Biomedical Microdevices, 2013. **15**(4):583-93

16. Gill, B.J., West, J.L., *Modeling the tumor extracellular matrix: Tissue engineering tools repurposed towards new frontiers in cancer biology.* Journal of Biomechanics, 2014. **47**(9):1969-78

17. Liu, H.W., et al., *Heterobifunctional Poly(Ethylene Glycol)–Tethered Bone Morphogenetic Protein-2–Stimulated Bone Marrow Mesenchymal Stromal Cell Differentiation and Osteogenesis.* Tissue Engineering, 2007. **13**(5):1113-24

18. Moon, J.J., et al., *Biomimetic hydrogels with pro-angiogenic properties.* Biomaterials, 2010. **31**(14):3840-7.

19. Delong, S.A., Gobin, A.S., West, J.L., *Covalent immobilization of RGDS on hydrogel surfaces to direct cell alignment and migration.* Journal of controlled release, 2005. **109**(1-3):139-48

20. Lee, A.L., et al., *Block copolymer mixtures as antimicrobial hydrogels for biofilm eradication.* Biomaterials, 2013. **34**(38):10278-86

21. Wang, C., Tong, X., Yang. F., *Bioengineered 3D brain tumor model to elucidate*

the effects of matrix stiffness on glioblastoma cell behavior using PEG-based hydrogels. Molecular Pharmaceuticals, 2014. **11**(7):2115-25

22. Singh, S.P., Schwartz, M.P., Lee, J.Y., Fairbanks, B.D., Anseth, K.S., *A peptide functionalized poly(ethylene glycol) (PEG) hydrogel for investigating the influence of biochemical and biophysical matrix properties on tumor cell migration.* Biomaterials Science, 2014. **2**(7):1024-1034.

23. Lee, A.L.Z., Ng, V.W.L., Gao, S., Hendrick, J.L., Yang, Y.Y., *Injectable Hydrogels from Triblock Copolymers of Vitamin E-Functionalized Polycarbonate and Poly(ethylene glycol) for Subcutaneous Delivery of Antibodies for Cancer Therapy.* Advanced Functional Materials, 2014. **21**(11): 1538-1550

24. Lo, C.M., et al., *Cell movement is guided by the rigidity of the substrate.* Biophysical journal, 2000. **79**(1):144-52.

25. Paszek, M.J., et al., *Tensional homeostasis and the malignant phenotype.* Cancer Cell, 2005. **8**(3):241-54.

26. Zhang. X., et al., *Development of an in vitro multicellular tumor spheroid model using microencapsulation and its application in anticancer drug screening and testing.* Biotechnology Progress, 2005. **21**(4):1289-96.

27. Ezquer, F., et al., *Mesenchymal stem cell therapy for doxorubicin*

cardiomyopathy: hopes and fears. Stem Cell Research and Therapy, 2015. **6**:116

28. Parthak, A., Kumar, S., *Transforming potential and matrix stiffness co-regulate confinement sensitivity of tumor cell migration.* Integrative Biology: quantative biosciences from nano to macro, 2013. **5**(8):1067-75

29. Fang, J.Y., et al., *Tumor Bioengineering Using a Transglutaminase Crosslinked Hydrogel*. PLoS One, 2014. **9**(8): e105616

30. Szot, C.S., Buchanan, C.F., Freeman, J.W., Rylander, M.N., *3D in vitro bioengineered tumors based on collagen I hydrogels.* Biomaterials, 2011. **32**(31):7905-12

31. Zheng, L., et al., *In vivo bioengineered ovarian tumors based on collagen, matrigel, alginate and agarose hydrogels: a comparative study.* Biomedical Materials, 2015. **10**(1):015016

Annex

1. Rheological Measurements

1.1 2.5% Collagen

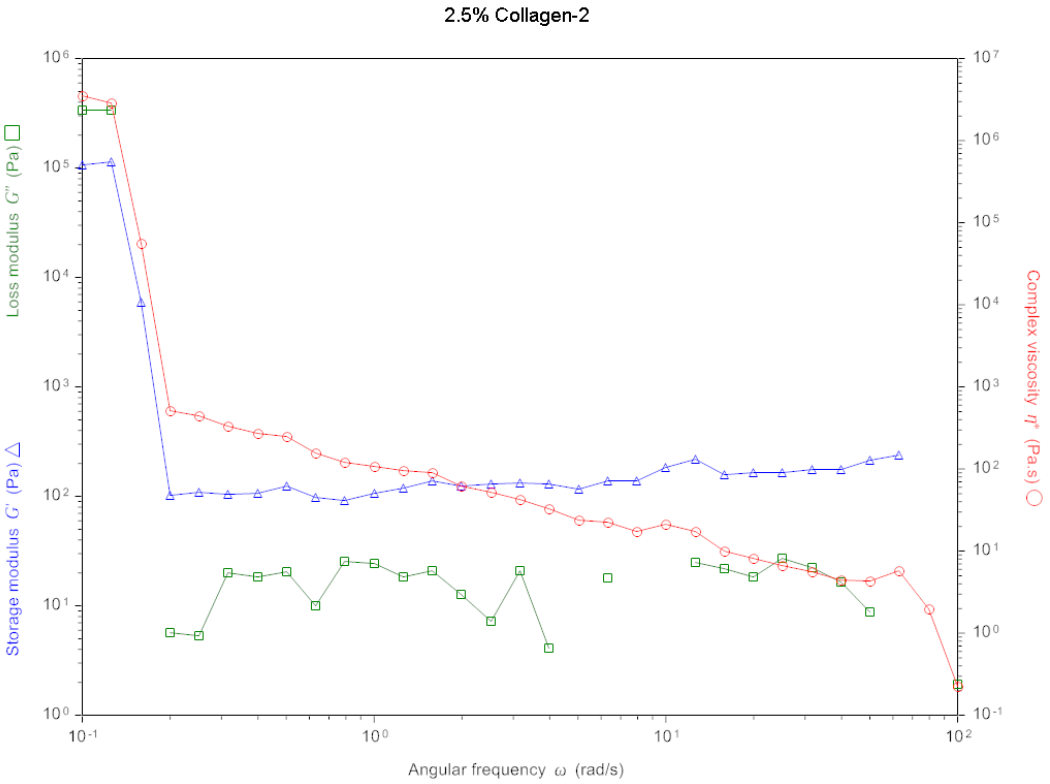

Angular frequency	Storage modulus	Loss modulus	Complex viscosity
rad/s	Pa	Pa	Pa.s
0.1	106501	341151	3573880
0.125893	113449	339634	2844340
0.158489	5964.05	-6688.42	56541.9
0.199526	102.533	5.73375	514.686
0.251189	110.084	5.33641	438.766
0.316228	103.36	19.9695	332.897
0.398107	107.081	18.4639	272.944
0.501187	124.107	20.5821	251.007
0.630957	98.6027	9.96859	157.071
0.794328	92.183	25.1872	120.305
1	106.131	24.6307	108.951
1.25893	119.818	18.3618	96.2863
1.58489	139.776	20.7696	89.1611
1.99526	123.421	12.5833	62.1779

2.51189	130.096	7.15242	51.8706
3.16228	133.171	20.7448	42.6203
3.98107	130.318	4.07152	32.7504
5.01187	117.187	-27.0875	23.9985
6.30957	139.83	18.0905	22.3462
7.94328	137.877	-6.29901	17.3758
10	181.769	-110.921	21.294
12.5893	217.575	24.9309	17.3957
15.8489	159.036	21.992	10.13
19.9526	163.74	18.5369	8.25884
25.1189	164.602	26.9399	6.64012
31.6228	175.726	22.1419	5.60087
39.8107	174.835	16.5251	4.41123
50.1187	213.205	8.73748	4.25757
63.0957	238.033	-269.33	5.69676
79.4328	-119.064	-105.061	1.99904
100	-22.5616	1.90376	0.226417

1.2 Polymer 2d 1.66mg/1.66%

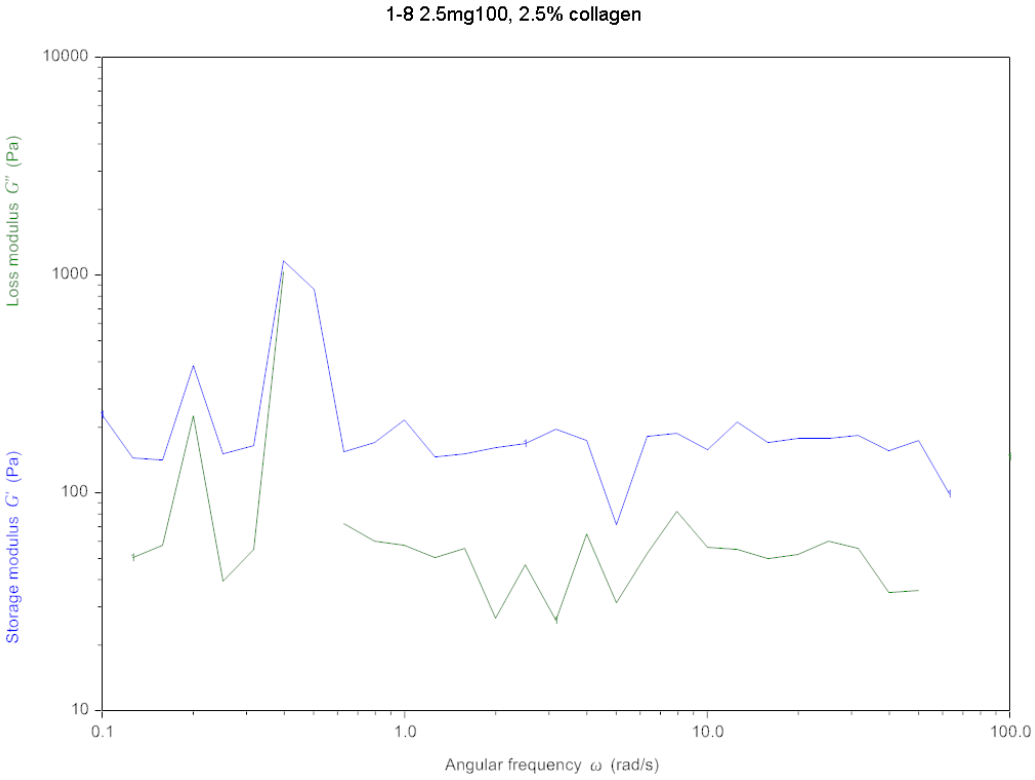

Angular frequency	Storage modulus	Loss modulus	Complex viscosity
rad/s	Pa	Pa	Pa.s
0.1	228.811	-193.551	2996.94
0.125893	143.994	50.3842	1211.79
0.158489	141.01	57.6236	961.137
0.199526	383.758	225.238	2230.16
0.251189	150.36	39.3953	618.798
0.316228	164.122	54.8714	547.239
0.398107	1170.25	1032.42	3919.98
0.501187	859.902	-871.674	2443.07
0.630957	155.124	72.3093	271.254
0.794328	170.182	59.9619	227.156
1	216.115	57.6831	223.681
1.25893	145.962	50.3958	122.658
1.58489	151.095	55.4929	101.561
1.99526	160.473	26.4416	81.5115
2.51189	167.688	46.7621	69.3048
3.16228	196.412	25.9435	62.6505
3.98107	173.327	64.9133	46.4909
5.01187	71.5608	31.3781	15.5906
6.30957	182.077	52.7273	30.0429
7.94328	187.55	82.1057	25.7746
10	157.906	56.1162	16.7581
12.5893	212.638	55.0622	17.4475
15.8489	170.788	49.6811	11.2227
19.9526	178.052	52.2585	9.30014
25.1189	178.188	60.1511	7.48707
31.6228	183.135	55.6061	6.05231
39.8107	156.435	34.8398	4.02574
50.1187	174.617	35.5023	3.55535
63.0957	98.4744	-132.061	2.61085
79.4328	-189.706	-37.1904	2.43372
100	-46.1827	146.095	1.53221

1.3 Polymer 2a, 1.66mg/1.66%

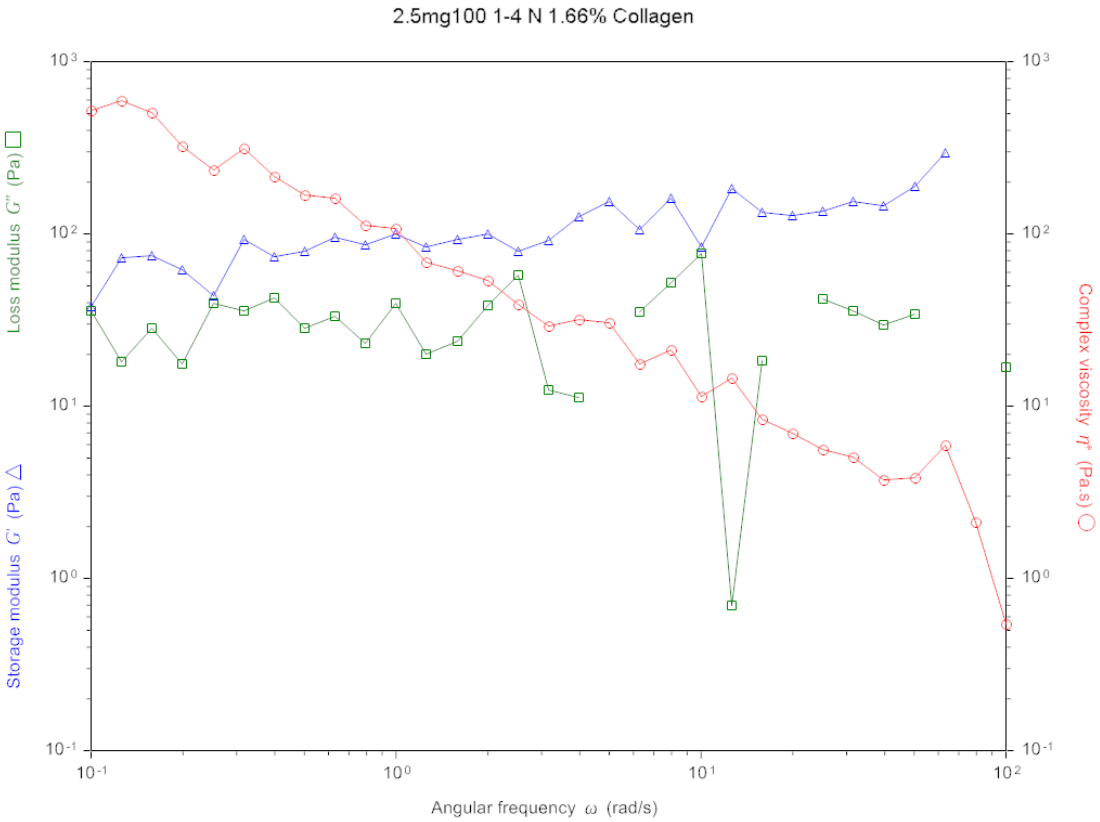

Angular frequency	Storage modulus	Loss modulus	Complex viscosity
rad/s	Pa	Pa	Pa.s
0.1	37.8601	35.7337	520.604
0.125893	72.6693	18.1151	594.898
0.158489	74.9378	28.4971	505.859
0.199526	61.8632	17.5927	322.344
0.251189	43.9178	39.3643	234.793
0.316228	92.754	35.9729	314.601
0.398107	74.1507	42.6598	214.883
0.501187	79.8299	28.2843	168.984
0.630957	96.0012	33.1767	160.981
0.794328	86.2601	23.2466	112.469
1	100.557	39.7036	108.112
1.25893	83.5494	20.0067	68.2419
1.58489	93.3482	23.7795	60.7797
1.99526	99.3203	38.3463	53.3593
2.51189	78.7892	57.9249	38.9312
3.16228	91.0904	12.4455	29.0729
3.98107	125.429	11.1959	31.6317
5.01187	153.522	-4.70185	30.646
6.30957	105.327	35.2765	17.6046

7.94328	160.443	52.0256	21.2339
10	84.0698	77.159	11.4111
12.5893	182.67	0.694387	14.5101
15.8489	132.652	18.4224	8.45012
19.9526	127.311	-53.5019	6.92118
25.1189	135.024	41.9391	5.62874
31.6228	155.223	35.9187	5.03827
39.8107	145.892	29.7727	3.74017
50.1187	188.224	34.4829	3.81807
63.0957	296.898	-226.891	5.92224
79.4328	-145.207	-84.1534	2.11285
100	-51.999	16.8318	0.546554

1.4 Polymer 2b, 1.66mg/1.66%

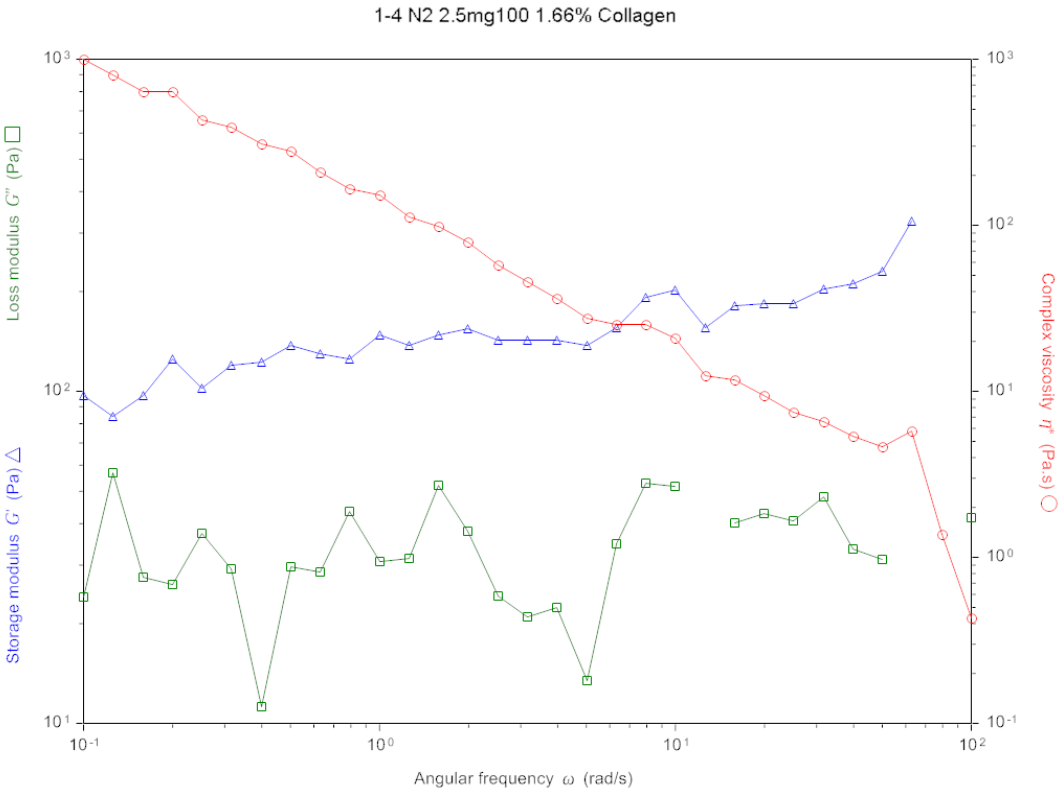

Angular frequency	Storage modulus	Loss modulus	Complex viscosity
rad/s	Pa	Pa	Pa.s
0.1	96.9235	24.0085	998.528
0.125893	84.0308	56.9817	806.472
0.158489	97.1363	27.5191	637.01
0.199526	125.521	26.2615	642.714
0.251189	102.467	37.2578	434.059
0.316228	120.251	29.1595	391.286

0.398107	122.808	11.2186	309.764
0.501187	137.835	29.6224	281.297
0.630957	129.882	28.5053	210.749
0.794328	124.95	43.5264	166.574
1	148.051	30.8295	151.227
1.25893	137.023	31.4634	111.674
1.58489	148.267	52.0737	99.1521
1.99526	154.219	37.8543	79.587
2.51189	142.928	24.2702	57.7151
3.16228	142.575	20.9013	45.5681
3.98107	143.05	22.3629	36.3689
5.01187	137.542	13.4625	27.5744
6.30957	155.62	34.6899	25.2694
7.94328	192.214	52.8842	25.0975
10	201.303	51.7336	20.7844
12.5893	155.609	-2.25665	12.3618
15.8489	180.732	40.1768	11.6818
19.9526	184.068	42.7357	9.47065
25.1189	183.961	40.646	7.50024
31.6228	203.301	47.9822	6.60558
39.8107	210.277	33.4885	5.34849
50.1187	230.106	31.1432	4.63308
63.0957	326.092	-167.271	5.80849
79.4328	-78.6263	-75.4145	1.37156
100	-12.4984	41.649	0.434839

1.5 Polymer 2c, 1.66mg/1.66%

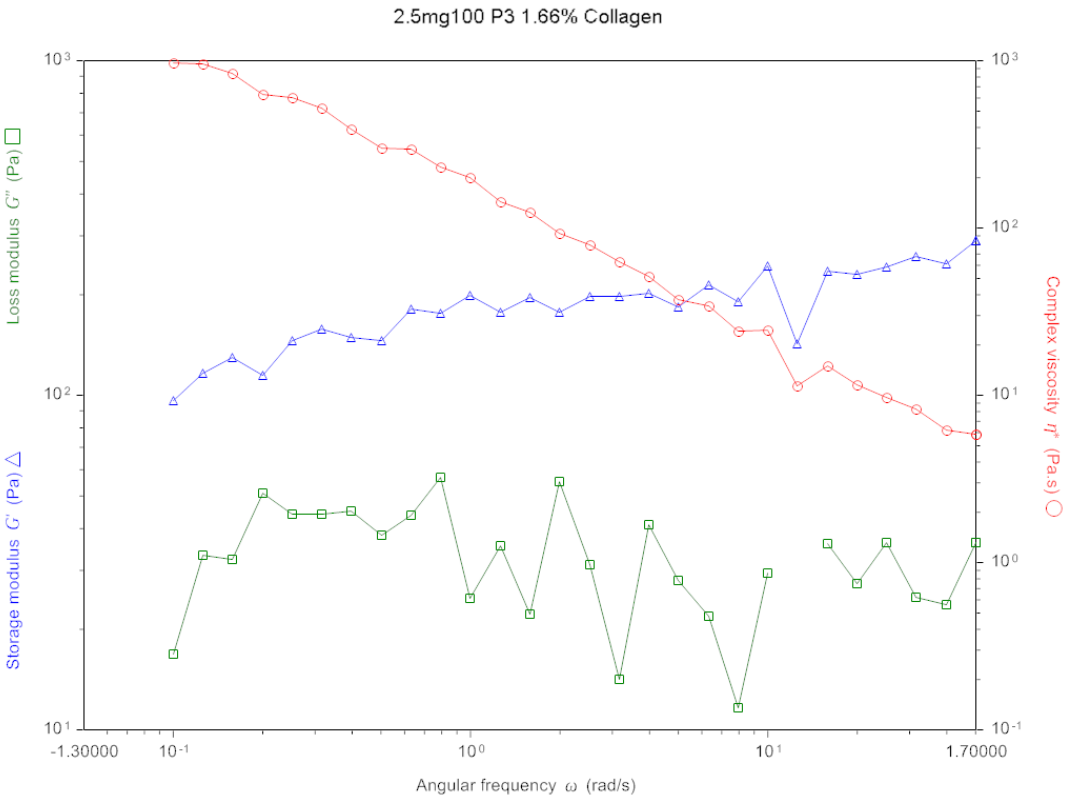

Angular frequency	Storage modulus	Loss modulus	Complex viscosity
rad/s	Pa	Pa	Pa.s
0.1	96.9235	24.0085	998.528
0.125893	84.0308	56.9817	806.472
0.158489	97.1363	27.5191	637.01
0.199526	125.521	26.2615	642.714
0.251189	102.467	37.2578	434.059
0.316228	120.251	29.1595	391.286
0.398107	122.808	11.2186	309.764
0.501187	137.835	29.6224	281.297
0.630957	129.882	28.5053	210.749
0.794328	124.95	43.5264	166.574
1	148.051	30.8295	151.227
1.25893	137.023	31.4634	111.674
1.58489	148.267	52.0737	99.1521
1.99526	154.219	37.8543	79.587
2.51189	142.928	24.2702	57.7151
3.16228	142.575	20.9013	45.5681
3.98107	143.05	22.3629	36.3689
5.01187	137.542	13.4625	27.5744
6.30957	155.62	34.6899	25.2694

7.94328	192.214	52.8842	25.0975
10	201.303	51.7336	20.7844
12.5893	155.609	-2.25665	12.3618
15.8489	180.732	40.1768	11.6818
19.9526	184.068	42.7357	9.47065
25.1189	183.961	40.646	7.50024
31.6228	203.301	47.9822	6.60558
39.8107	210.277	33.4885	5.34849
50.1187	230.106	31.1432	4.63308
63.0957	326.092	-167.271	5.80849
79.4328	-78.6263	-75.4145	1.37156
100	-12.4984	41.649	0.434839

1.6 Polymer 2c 2.3mg/1.66%

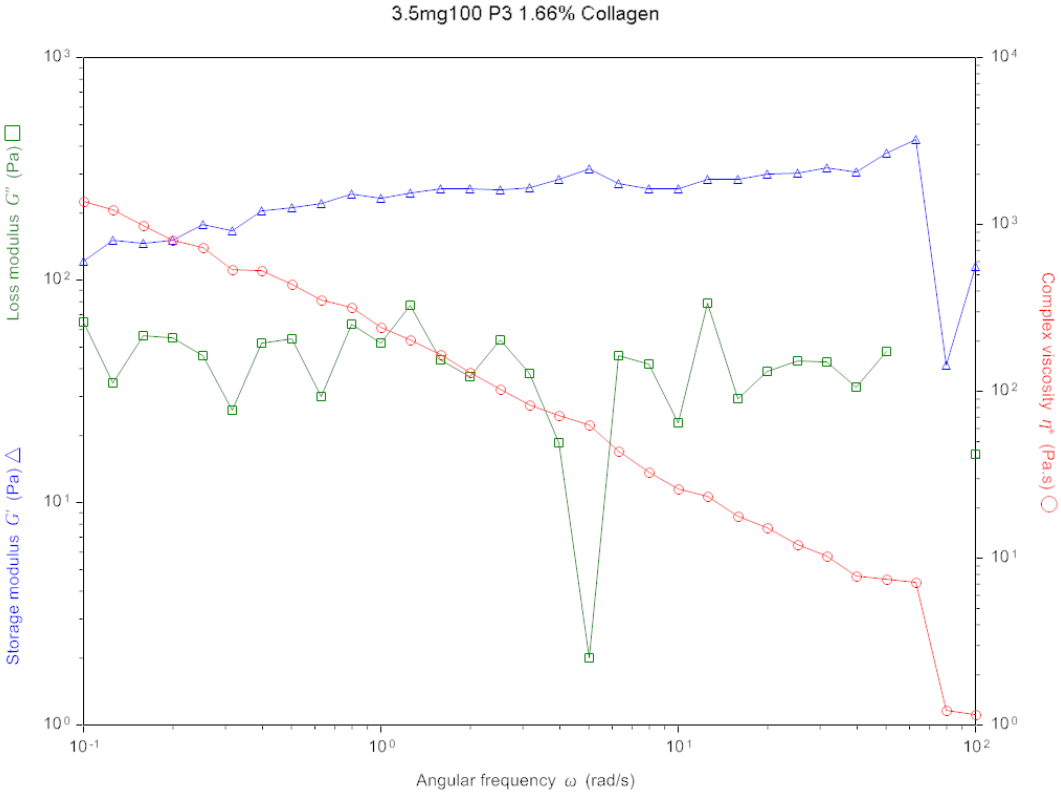

Angular frequency	Storage modulus	Loss modulus	Complex viscosity
rad/s	Pa	Pa	Pa.s
0.1	122.016	64.7819	1381.47
0.125893	151.343	34.6215	1233.21
0.158489	146.74	56.2436	991.544
0.199526	151.098	54.911	805.741
0.251189	177.269	45.7341	728.829
0.316228	166.992	26.0263	534.451
0.398107	204.36	52.3629	529.912

0.501187	211.226	54.1369	435.074
0.630957	219.927	29.9303	351.774
0.794328	244.045	63.6763	317.52
1	234.468	52.0402	240.173
1.25893	246.114	76.7562	204.782
1.58489	258.113	43.9517	165.202
1.99526	257	36.7306	130.114
2.51189	254.691	53.9862	103.647
3.16228	260.79	37.8314	83.3321
3.98107	284.001	18.5172	71.4892
5.01187	314.681	2.01355	62.7884
6.30957	272.671	45.9016	43.8235
7.94328	258.463	42.1543	32.9685
10	257.87	22.773	25.8874
12.5893	284.691	78.4234	23.4561
15.8489	282.658	29.3403	17.9304
19.9526	300.781	38.6778	15.1989
25.1189	301.329	43.3004	12.1194
31.6228	320.894	42.8947	10.2378
39.8107	307.561	33.1233	7.77026
50.1187	371.774	48.0154	7.47947
63.0957	426.849	-151.652	7.17938
79.4328	41.6718	-88.0989	1.22692
100	114.859	16.5137	1.1604

1.7 Polymer 2c 3.3mg/1.66%

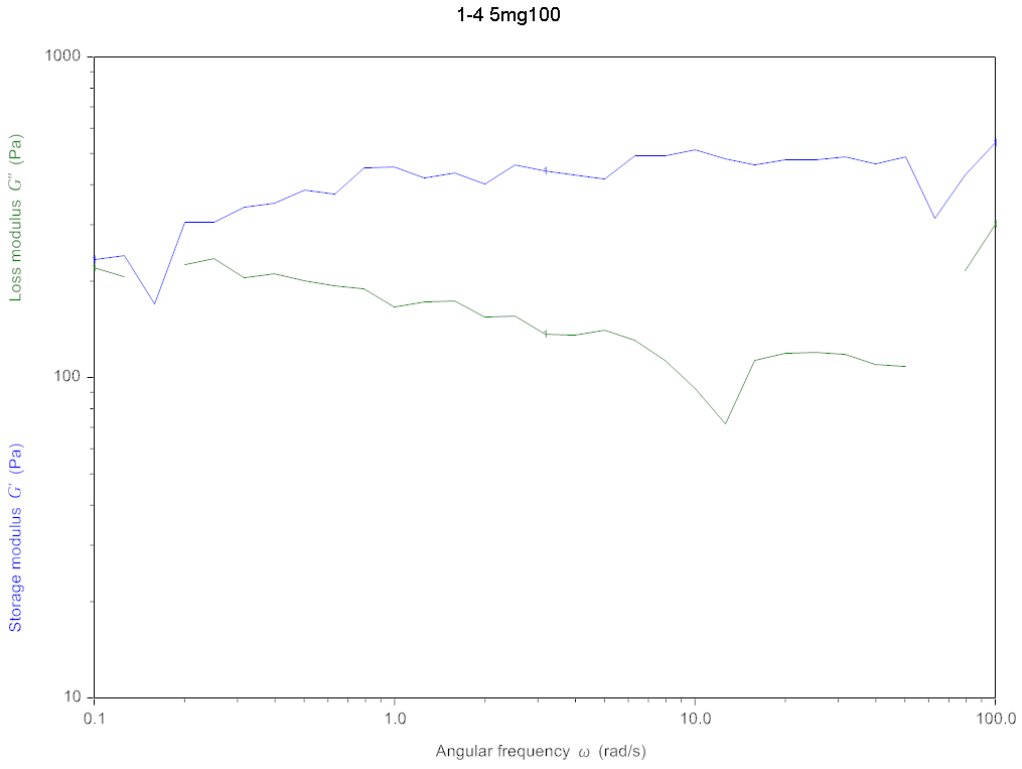

Angular frequency	Storage modulus	Loss modulus	Complex viscosity
rad/s	Pa	Pa	Pa.s
0.1	232.712	220.169	3203.58
0.125893	240.793	206.375	2519.06
0.158489	169.506	-152.473	1438.53
0.199526	304.418	225.123	1897.58
0.251189	304.623	235.562	1533.02
0.316228	339.637	205.044	1254.58
0.398107	348.835	210.933	1023.97
0.501187	384.515	200.911	865.624
0.630957	374.699	193.447	668.332
0.794328	451.494	189.5	616.433
1	454.762	166.186	484.176
1.25893	419.995	171.522	360.362
1.58489	436.21	173.482	296.197
1.99526	402.769	154.716	216.243
2.51189	462.136	156.06	194.187
3.16228	442.42	136.08	146.374
3.98107	428.212	135.37	112.809
5.01187	415.066	140.164	87.4111
6.30957	490.273	130.836	80.4223
7.94328	492.625	113.155	63.6328
10	511.829	92.4637	52.0114
12.5893	479.963	71.6487	38.5473
15.8489	462.234	112.826	30.0212
19.9526	477.342	119.344	24.6602
25.1189	477.805	119.99	19.6124
31.6228	486.838	118.417	15.844
39.8107	465.033	110.097	12.004
50.1187	489.11	108.418	9.99591
63.0957	313.45	-146.01	5.48038
79.4328	428.257	216.063	6.03874
100	541.103	300.061	6.18732

1.8 Polymer 1, 1.25mg/1.66%

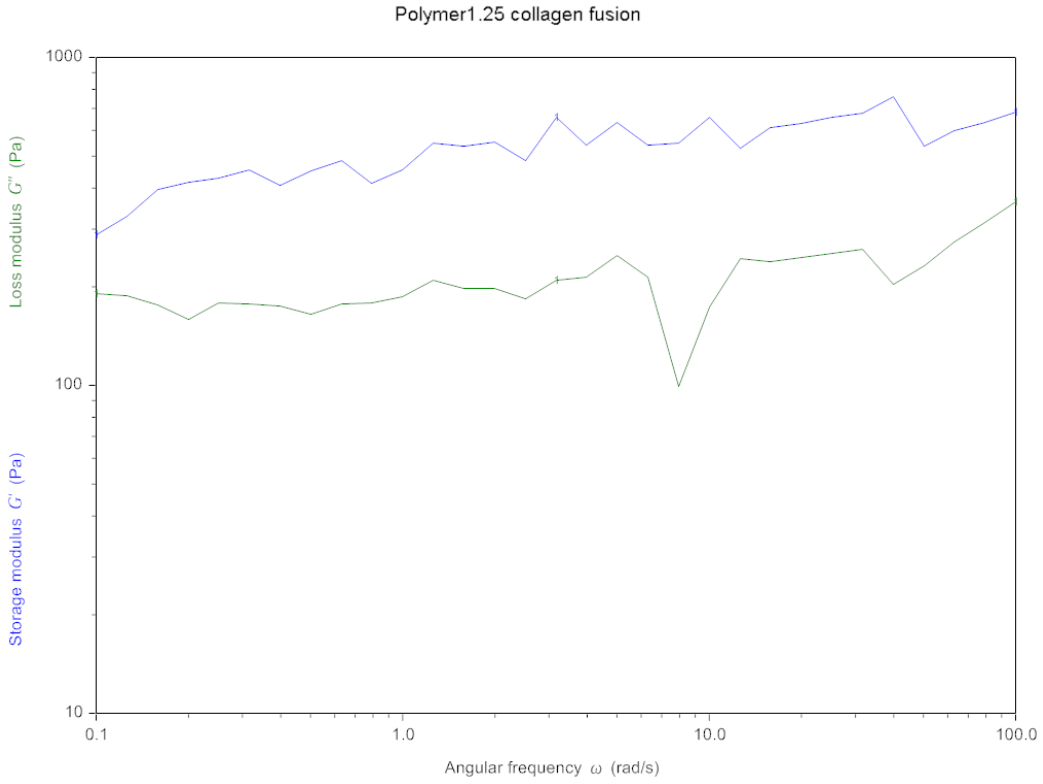

Angular frequency	Storage modulus	Loss modulus	Complex viscosity
rad/s	Pa	Pa	Pa.s
0.1	286.906	189.857	3440.36
0.125893	327.044	188.38	2997.94
0.158489	395.61	176.025	2732.07
0.199526	417.888	159.245	2241.32
0.251189	428.109	179.012	1847.33
0.316228	452.985	177.817	1538.88
0.398107	406.369	175.264	1111.64
0.501187	450.021	165.307	956.573
0.630957	483.23	177.032	815.645
0.794328	414.366	178.187	567.844
1	454.037	186.53	490.86
1.25893	547.227	210.013	465.589
1.58489	535.839	197.053	360.228
1.99526	553.185	198.04	294.48
2.51189	483.391	183.757	205.877
3.16228	657.136	210.031	218.161
3.98107	541.655	214.094	146.3
5.01187	634.925	248.223	136.021
6.30957	541.083	213.117	92.168
7.94328	549.79	99.4161	70.337

10	658.491	173.885	68.1063
12.5893	528.154	243.454	46.1952
15.8489	610.89	239.012	41.3897
19.9526	630.534	245.441	33.9113
25.1189	656.429	252.205	27.9954
31.6228	678.135	260.255	22.9695
39.8107	760.298	203.92	19.7728
50.1187	536.398	231.842	11.6595
63.0957	598.981	274.253	10.441
79.4328	631.64	314.316	8.88202
100	683.518	361.646	7.73294

2. Spheroid Growth Data

2.1 Hydrogel encapsulated spheroid growth over seven days

2.5% Collagen						
Day 1	**Day 2**	**Day 3**	**Day 4**	**Day 5**	**Day 6**	**Day 7**
222.52	229.213	231.713	238.671	235.289	242.739	258.96
240.256	243.469	238.292	251.428	260.554	258.451	264.763
226.28	231.145	248.395	265.861	260.583	264.582	262.901
300.25	310.505	328.456	340.541	360.984	363.774	403.445
232.56	238.053	245.254	265.465	285.82	290.401	302.227
312.247	314.667	335.425	289.587	423.66	444.381	438.254
328.25	334.555	339.682	339.482	341.107	351.146	362.724
278.56	286.355	310.44	361.114			
244.56	246.865	268.481	300.015			

1.66% Collagen/1.6mg Polymer 2a						
Day 1	**Day 2**	**Day 3**	**Day 4**	**Day 5**	**Day 6**	**Day 7**
284	292	291	294	299	301	301
213	230	229	237	255	252	256
240	260	267	267	272	275	279
199	196	213	209	232	240	243
275	275	280	273	275	280	289
274	279	279	280			
171	175	167	168			
142	135					
225		247				
244		267				

246		252				
271		282				
184		193				
238		263				

1.66% Collagen/1.6mg Polymer 2b						
Day 1	**Day 2**	**Day 3**	**Day 4**	**Day 5**	**Day 6**	**Day 7**
263.691	274.905	258.235	276.358	273.821		289
298.31	300.746	306.725	301	312		335
194.349	199.532	208	212.441	218		228
215	239	234	235	240	248	275
242	266	252	260	268	272	289
213	238	234	219	226	229	240
253	278	269	264	268	272	284
186		199	202	206	211	219
147		180	164	165	168	183
165		186	192	199	224	222

1.66% Collagen/1.6mg Polymer 2c						
Day 1	**Day 2**	**Day 3**	**Day 4**	**Day 5**	**Day 6**	**Day 7**
314.556	338.457	368.525	391.908	401.584	408.148	416.992
110.856	118.692	112.554	127.425	139.541	152.05	150.241
272.586	275.992	277.55	281.555	285.541	290.08	289.945
265.578	273.544	285.547	297.494	312.544	356.53	363.364
205.547	225.456	235.78	246.786	254.544	265.08	279.558
256.855	254.743	251.922				
250.288	303.862	285.291				

267.456	304.797	311.142				
278.007	313.497	344.98				

1.66% Collagen/1.6mg Polymer 2d						
Day 1	**Day 2**	**Day 3**	**Day 4**	**Day 5**	**Day 6**	**Day 7**
242.56	247.936	247.687	245.424	280.796	280.579	279.528
238.58	239.709	239.582	239.709	238.29	245.578	247.285
266.524	266.257	268.268	268.554	263.213	265.547	270.056
252.525	255.133	259.586	263.558	259.865	267.169	285.996
221.358	221.88	226.548	231.984	237.38	241.548	247.58
224.856	233.554	248.589	242.99	246.548	253.332	264.778
244.582				239.191	244.586	249.547
220.542			214.701	217.915	224.225	226.548

1.66% Collagen/3.3mg Polymer 2d						
Day 1	**Day 2**	**Day 3**	**Day 4**	**Day 5**	**Day 6**	**Day 7**
248.92	249.921	266.637	255.114	262.619	265.205	263.923
264.58	269.684	272.068	279.954	277.727	278.784	269.22
270.58	272.688	264.348	267.424	257.362	251.73	248.769
267.58	268.791	274.15	291.025	280.736	244.124	240.985
328.58	323.119	305.839	302.791	305.858	304.445	309.737
248.52	252.326	283.353	278.757	282.455	289.414	295.935
245.25	250.085	267.72	292.341	314.454	329.44	344.844
270.24	282.132	280.26	305.859			

2.2 Spheroid growth after doxorubicin treatment (IC50)

1.66% Collagen/1.6 mg Polymer 2c						
Day 1	**Day 2**	**Day 3**	**Day 4**	**Day 5**	**Day 6**	**Day 7**
285.527	307.423	332.304	324.304	352.511	350	346.88
263.207	292.812	290.972	295.883	314.43	315.65	314.67
268.12	291.784	300.622	317.985	328.49	330.13	339.34
233.132	249.586	265.098	279.415	321.483	323.554	330.087
303.916	329.262	342.865	374.356	380.471	378.58	373.184
272.12	293.784	304.622	319.985	325.49	332.13	341.34

1.66% Collagen/1.3 mg Polymer 2c						
Day 1	**Day 2**	**Day 3**	**Day 4**	**Day 5**	**Day 6**	**Day 7**
292.106	300.706	316.757	323.448	335.055	341.638	344.969
242.523	238.127	234.604	227.79	230.18	231.341	228.979
291.659	295.873	301.528	305.291	301.741	312.317	313.59
256.115	284.828	287.405	297.991	305.737	318.899	323.563
317.257	326.425	329.47	330.176	330.645	330.648	341.241
282.012	288.345	290.946	338.635	353.914	361.665	368.021
293.751	291.878	310.672	319.839	322.189	321.502	330.71
308.098	315.136	322.677	325.24	339.107	336.99	341.706
285.774	276.838	284.825	322.656	338.636	340.758	346.159
317.25	310.905	323.174	354.154	358.386	354.154	355.559
313.971	325.711	331.117	331.585	337.461	348.741	354.635
289.05	299.641	305.974	326.181	329.705	329.47	329.24

2.5% Collagen (DOX)						
Day 1	**Day 2**	**Day 3**	**Day 4**	**Day 5**	**Day 6**	**Day 7**
224.892	235.593	238.783	237.862	257.565	257.565	264.852
198.593	206.589	207.27	209.642	209.161	208.685	216.441
220.195	181.211	192.936	191.764	191.781	195.575	196.674
204.222	200.221	219.038	230.312	227.482	232.25	237.153
226.07	249.573	251.451	252.411	244.649	245.25	250.04
234.369	268.135	263.201	269.078	263.224	268.57	271.428
241.348	260.387	262.754	265.315	266.498	264.586	265.315
204.933	230.771	239.938	235.004	228.67	228.596	229.83
274.184	285.336	289.978	300.047	311.64	312.496	310.363
280.261	297.791	317.25	334.235	333.029	334.586	337.254
108.79	123.809	142.148	162.198	169.044	165.156	160.769

Non-gel Spheroids (DOX)						
Day 1	**Day 2**	**Day 3**	**Day 4**	**Day 5**	**Day 6**	**Day 7**
294.221	273.776	261.5	254.273	258.975	237.82	218.431
271.428	271.9	261.56	225.838	246.335	224.425	202.191
284.162	278.945	249.61	238.776	236.645	210.618	223.251
262.735	286.94	269.318	250.513	248.164	216.437	215.266
259.205	259.461	234.6	249.335	208.246	225.375	216.08
265.32	285.29	253.097	250.523	243.963	240.897	238.806
288.815	269.076	274.488	255.683	249.371	227.519	
269.31	303.388	261.331	254.27	264.848	247.703	
282.94	274.534	250.989	233.356	224.666	225.375	
272.366	255.488	251.688	255.933	241.345	243.704	
285.29	274.488	252.181	243.46	236.175	216.44	

288.376	273.075	268.137	245.81	251.45	221.141	

1.66% Collagen/1.6mg Polymer 2a						
Day 1	**Day 2**	**Day 3**	**Day 4**	**Day 5**	**Day 6**	**Day 7**
284	292	291	294	299	301	301
213	230	229	237	255	252	256
240	260	267	267	272	275	279
199	196	213	209	232	240	243
275	275	280	273	275	280	289
274	279	279	280	285	289	290
171	175	167	168	170	175	179

2.3 Spheroid growth rate at day 7 after Doxorubicin treatment

Hydrogel Composition	Equatorial Diameter							Polar Diameter						
	Day 1	Day 2	Day 3	Day 4	Day 5	Day 6	Day 7	Day 1	Day 2	Day 3	Day 4	Day 5	Day 6	Day 7
Free spheroid (Control)	263	283	308	328		351	351	285	299	272	287		302	340
	268	263	273	296		327	342	245	269	275	314		322	333
	259	254	307	332		346	372	276	291	261	288		298	317
Dox Free IC50X5 (Collagen 2.5%)	298	290		293		287	283	286	286		301		289	289
	329	323		306		296	299	224	263		253		234	232
	151	145		140		135	130	253	248		244		240	240
Dox/B+U Mixed Micelle IC50X5 (Collagen 2.5%)	324	305	272	278		272	275	227	180	176	207		192	202
	223	207	205	200		196	199	332	308	303	298		294	289
	167	181	155	156		156	156	334	335	310	305		304	302
Dox Free IC50X5 (1.66% Collagen/1.6mg Polymer 2c)	247	279	274	268		264	231	310	336	324	347		343	366
	308	313	295	293		286	287	314	313	295	291		282	285
	332	341	292	304		301	299	260	271	241	244		248	250
Dox B+U Mixed Micelle IC50X5 (1.66% Collagen/1.6 mg Polymer 2c)	163	162	188	197		195	187	259	243	246	258		258	255
	193	180	182	183		170	193	305	295	284	311		283	274
	286	229	210	201		195	192	308	318	284	280		261	261

3 Cell viability data

	Absorbance								
Polymer 2d 1.6mg/1.66% Collagen	0.9412	0.9460	0.8501	1.2648	0.9354	0.9582	0.8460		
Polymer 2a 1.6mg/1.66% Collagen	0.6848	0.4550	0.5311	0.5429	0.5690	0.8548	0.7789	0.8704	0.7867
2.5% Collagen	0.8590	0.5307	0.6948	1.1356	0.6825	0.7204	0.5834		
2D Cell Culture	0.4987	0.5344	0.5132	0.4790	0.6110	0.5364	0.5429	0.4776	